

# Deep Networks Learn to Parse Uniform-Depth Context-Free Languages from Local Statistics

Jack T. Parley<sup>1</sup> Francesco Cagnetta<sup>2</sup> Matthieu Wyart<sup>3</sup>

## Abstract

Understanding how the structure of language can be learned from sentences alone is a central question in both cognitive science and machine learning. Studies of the internal representations of Large Language Models (LLMs) support their ability to parse text when predicting the next word, while representing semantic notions independently of surface form. Yet, which data statistics make these feats possible, and how much data is required, remain largely unknown. Probabilistic context-free grammars (PCFGs) provide a tractable testbed for studying these questions. However, prior work has focused either on the post-hoc characterization of the parsing-like algorithms used by trained networks; or on the learnability of PCFGs with fixed syntax, where parsing is unnecessary. Here, we (i) introduce a tunable class of PCFGs in which both the degree of ambiguity and the correlation structure across scales can be controlled; (ii) provide a learning mechanism—an inference algorithm inspired by the structure of deep convolutional networks—that links learnability and sample complexity to specific language statistics; and (iii) validate our predictions empirically across deep convolutional and transformer-based architectures. Overall, we propose a unifying framework where correlations at different scales lift local ambiguities, enabling the emergence of hierarchical representations of the data.

## 1. Introduction

How languages are learned is a central question of linguistics. The celebrated “poverty of the stimulus” argument (Chomsky, 1980) questioned whether learning from

<sup>1</sup>Institute of Physics, EPFL <sup>2</sup>Theoretical and Scientific Data Science, SISSA <sup>3</sup>Department of Physics and Astronomy, Johns Hopkins University (On leave from EPFL). Correspondence to: Jack T. Parley <jack.parley@epfl.ch>.

Preprint. February 9, 2026.

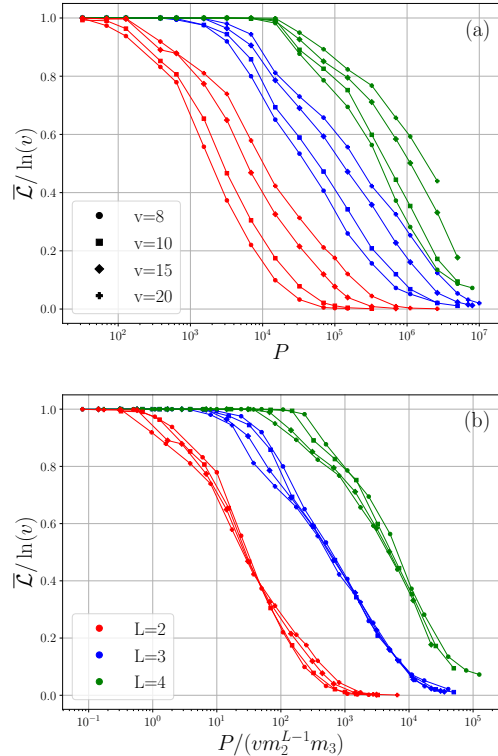


Figure 1. (a) Test cross-entropy loss  $\bar{L}$  (normalized by random guessing) of a deep CNN as a function of the number of training sentences  $P$ , generated from a varying-tree PCFG of uniform depth  $L$  and vocabulary size  $v$ . (b) Remarkably, curves collapse when  $P$  is rescaled by our theoretical prediction for sample complexity.  $m_2$  and  $m_3$  characterize the number of production rules (see main text), here  $m_2$  is constant and  $m_3 \propto v$ .

examples alone was even possible, and led to the proposition that grammar is innate. The distributional approach, instead, posited that the statistics of the input data are sufficient to deduce the language structure (Ellis, 2002; Saffran & Kirkham, 2018; Saffran et al., 1996)—a possibility later established by the advent of Large Language Models (LLMs) (Devlin et al., 2019; Radford et al., 2018). Understanding the reasons for their success, however, remains a central challenge. Studies of internal representations of LLMs indicate that (i) they parse text (Peters et al., 2018; Tenney et al., 2019; Manning et al., 2020; Diego-Simón

et al., 2024) and (ii) they build representations of semantic notions, such as the “Golden Gate Bridge” (Templeton et al., 2024; Gurnee et al., 2026), which are extremely robust toward variations in syntax. The mechanism whereby these two feats are learned is however essentially unknown, including which correlations in text are exploited, and how much training data is required to do so.

Inspired by the symbolic generative approach (Chomsky, 1957), probabilistic context-free grammars (PCFGs) provide a powerful tool to model languages and to study the questions above quantitatively. In these models, a tree of latent (or “nonterminal”) variables underlies the text structure. These latent variables can be used to model syntax, but also abstract semantic notions. The classic bottom-up method to parse a PCFG is the inside algorithm (Baker, 1979), a sum-product algorithm which recursively computes the probability of latent symbols deriving spans of a sentence. Recent works have shown that transformers approximately implement the inside algorithm (Allen-Zhu & Li, 2025; Zhao et al., 2023) and can perform context-free recognition (Jerad et al., 2026), but do not address how such algorithms are learned during training nor how much data is needed.

A strategy to study learnability (Clark, 2017) is to consider synthetic PCFGs of controlled structure (Malach & Shalev-Shwartz, 2018; Mossel, 2016). In (Cagnetta et al., 2024), the Random Hierarchy Model (RHM) was introduced, a fixed-tree PCFG where production rules (describing how latent variables generate strings of other variables) are chosen randomly. The mechanism for how deep networks learn such data and the associated sample complexity were elucidated for supervised learning (Cagnetta et al., 2024), next token prediction (Cagnetta & Wyart, 2024) and diffusion models (Favero et al., 2025): strings of tokens that correlate with the tasks are grouped together, in a recursive manner, allowing the network to reconstruct the tree of latent variables hierarchically. If production rules are not random but fine-tuned to remove these correlations, learning becomes virtually impossible in high dimensions (Cagnetta et al., 2024); showing that the learnability of worst and typical cases differ. A central limitation of these works is that they consider fixed trees—syntax is frozen, and parsing is not necessary. Removing the fixed-topology assumption profoundly changes the learning problem: (A) learners need to decipher which span of the text corresponds to a given latent variable, and (B) ambiguity appears, where the same substring of the sentence could have been generated by different latent variables.

## 1.1. Our contribution

(i) We introduce a family of synthetic grammars with random production rules and varying trees, obtained by letting

production rules generate strings of different lengths. Although the number of parse trees grows exponentially with the full sentence length, we show that global ambiguity (having multiple parse trees with different root labels per sentence) is controlled by a transition that depends on the number of production rules. This property allows us to have detailed control of the level of ambiguity.

(ii) We provide a mechanism for learning the root classification task (and discuss the implications of our findings for next-token prediction in the conclusion), in the form of an algorithm that can learn the production rules so as to parse sentences into a hierarchical tree of latent variables. This analysis shows that iterative clustering based on correlations (Malach & Shalev-Shwartz, 2018; Cagnetta et al., 2024) to identify latent variables can overcome problems (A) and (B). It predicts that the sample complexity scales as a power law of the number of production rules and vocabulary size, corresponding to the minimal sample size where correlations between the root and substrings of adjacent tokens can be measured precisely.

(iii) We test these predictions empirically in the regime of low global ambiguity, typical of natural languages, both for deep CNNs and transformers, and confirm our predictions quantitatively.

## 1.2. Previous works

**Languages with random rules:** In (DeGiuli, 2019), it was shown that a transition toward fully structureless, noisy languages can take place. In (Hsu et al., 2012) the impossibility of learning was established under similar conditions.

**Learning PCFGs** is a classic example of learning a latent-variable probabilistic model. The standard approach relies on maximum likelihood and expectation-maximization (EM) (Dempster et al., 1977), involving iterative re-estimation of rule probabilities (Baker, 1979; Pereira & Schabes, 1992; Klein & Manning, 2004). However, the application of EM to infer a PCFG offers no guarantees of convergence to global minima (Balle et al., 2014). Of particular relevance for us is the “hard” setting, where training data does not include parse trees. Progress in this setting is limited: (Bailly et al., 2013) cast PCFG inference as a low-rank factorization, which however leads to an intractable optimization problem, while (Clark & Yoshinaka, 2013) showed that substitutable context-free languages are identifiable in the large samples limit from positive examples, but neither provide finite sample complexity guarantees. (Cohen & Smith, 2012) give a bound on sample complexity if some optimizer is found, but they show that this optimization is NP hard in general. This motivates the introduction of our controlled synthetic PCFGs, which allow to extract quantitative predictions of sample complexity even in the “hard” setting.

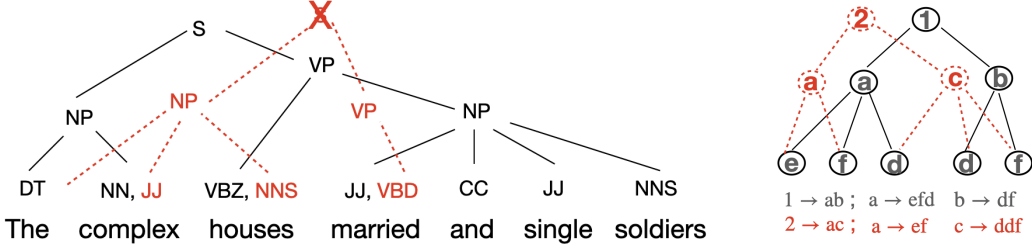


Figure 2. Left: local vs. global ambiguity (both lexical and syntactic) in natural language. In this “garden-path” sentence (Frazier & Rayner, 1982), the reader is pushed by habit into reading *the complex houses* as a noun phrase (NP); pursuing this, however, leads to a dead end (an incomplete parse) so that the sentence remains globally unambiguous. Right: example of global ambiguity in a varying-tree RHM of depth  $L = 2$ , where the sentence “efddf” has two associated parse trees/class labels. Shown below are the production rules used in each case to derive the sentence.

## 2. Varying-tree Random Hierarchy Model

### 2.1. Generative Model

PCFGs are fully defined by specifying both the set of symbols and their production rules. Symbols can be visible (“terminal”) or latent (“nonterminal”). Only the latter produce strings of symbols. Here we consider a family of uniform-depth PCFGs, whose trees always have the same depth, with the following properties:

(1)  $L+1$  finite vocabularies  $(\mathcal{V})_{l=0,\dots,L}$ , where  $\mathcal{V}_0$  denotes a set of  $n_c$  class labels or root symbols.  $\mathcal{V}_L$  instead denotes the set of terminal symbols or tokens which form the generated sentence. For simplicity, we consider a fixed vocabulary size  $v$  of nonterminals across layers, including class labels  $n_c=v$ .

(2) For each level- $l$  symbol, we sample without replacement (and uniformly at random)  $m_2$  binary rules and  $m_3$  ternary rules, corresponding respectively to tuples of  $s = 2, 3$  level- $(l+1)$  symbols. These production rules are unambiguous: two distinct nonterminals cannot generate the same tuple. To derive a sentence, we first pick a root symbol with uniform probability, and then apply the rules iteratively (layer by layer) to rewrite each level- $l$  symbol in terms of level- $(l+1)$  symbols (see an example in Fig. 2 right), until the (level- $L$ ) tokens form a sentence. Given branching ratios of equal probability  $p_2=p_3=1/2$ , normalization of the PCFG and assuming for simplicity uniformity across rules (relaxing this hypothesis does not affect our theoretical approach, see below), this implies that each binary rule can be picked with probability  $1/(2m_2)$ , and each ternary rule with probability  $1/(2m_3)$ .

(3) When we consider the asymptotic limit  $v \rightarrow \infty$ , the number of rules follows  $m_2 = f_2 v$  and  $m_3 = f_3 v^2$ . Although the theory applies more generally, we often test the model with  $f_2=f_3=f$ . In this case, if we consider a randomly chosen binary (or ternary) tuple from the total of  $v^2$  (or  $v^3$ ) such tuples, it will correspond to a grammatical rule with probability  $f$ .

To understand why, even though the rules themselves are unambiguous, multiple branching ratios nonetheless lead to syntactic ambiguity, consider the following. If we fix a ternary rule  $\{abc\}$  belonging to the grammar, with probability  $f$  there will also be a grammatical binary rule reading as  $\{ab\}$  (or equivalently,  $\{bc\}$ ). If this is the case, then the substring  $(abc)$  can appear *fortuitously* in the output sentence if the binary rule  $\{ab\}$  is followed by a rule (of either type) starting by  $c$ , which occurs with a probability of  $\mathcal{O}(1/v)$ . Importantly, the overall probability of this fortuitous occurrence is then  $\sim 1/(2vm_2) = 1/(2m_3)$ , i.e. of the same order as the genuine occurrence, making the grammar (at least) locally ambiguous.

For such combinatorial generative models, it is clear that the number of generated sentences grows exponentially with the input dimension (sentence length)  $d$  (Cagnetta et al., 2024). It is also straightforward to study analytically the depth-dependence of key properties, such as the distribution controlling the fluctuations in sentence length or the total number of tree topologies. These are given in detail in App A. In brief, sentence lengths at depth  $L$  are broadly distributed around the typical value  $d \sim \langle s \rangle^L$ , with the average branching ratio  $\langle s \rangle = 2.5$ . A second key quantity is the number of topologically possible parse trees for a sentence of length  $d$  at depth  $L$ , which also grows exponentially with the typical length as  $N_t(\langle s \rangle^L, L) \sim 2^{(\langle s \rangle^L - 1)/(\langle s \rangle - 1)}$ .

### 3. Controlling the level of global ambiguity

Given this combinatorial explosion of parse trees, do sentences generated by an instance of the varying-tree RHM remain globally unambiguous? By global ambiguity, we refer to whether, given a sentence  $x$  one can assign to it a unique class label  $\alpha(x)$ . This is analogous to the notion of global ambiguity in linguistics, where the existence of multiple parse trees deriving the same sentence is associated to multiple interpretations or meanings (Fig. 2).

To study this question quantitatively, we turn to the classic inside parsing algorithm (Baker, 1979), a dynamic program-

ming algorithm. Given a PCFG defined by its rule probabilities, and a sentence  $x$ , it computes the probability  $Pr(x)$  of the sentence within the language. To do so, it sums over the set of all grammatical parse trees  $T$  of  $x$ , denoted by  $\mathcal{T}(x)$ . Each of these contributes through the conditional  $Pr(x|T)$ , given in turn by the product of probabilities of all rules appearing on the tree  $T$ .

To study the classification task of the  $v$  labels  $\alpha$  that act as root symbols, it is useful to define  $\mathcal{T}_\alpha(x)$  as the subset of grammatical parse trees with root symbol  $\alpha$ . From this subset one computes  $Pr(x|\alpha) = \sum_{T \in \mathcal{T}_\alpha(x)} Pr(x|T)$  from which we can obtain the conditional probability over class labels  $Pr(\alpha|x) = Pr(x|\alpha)/(vPr(x))$ . Here we used that class labels  $Pr(\alpha) = 1/v$  are equally probable. From this quantity, we can compute the conditional *class entropy* given a sentence  $x$ ,  $H(\alpha|x)$ , that characterizes the global ambiguity of that sentence.

**The inside algorithm** is explained in detail in App. B. It proceeds by computing *inside probabilities* of nonterminals “anchored” to a span (i.e. substring) of the sentence (Goodman, 1996). In particular, we define a span by its start position  $i$  and span length  $\lambda$ . The inside probabilities then correspond to the probabilities  $Pr(x_i \dots x_{i+\lambda-1}|z)$  that the non-terminal  $z$  “yields” the substring  $x_i \dots x_{i+\lambda-1}$ . They can be stored in an *inside tensor*  $M_{i,\lambda}(z)$ , in general of shape  $d \times d \times v$ . For a uniform-depth grammar as considered here (see Fig. 4), we can construct  $l = L, \dots, 0$  separate tensors  $M_{i,\lambda}^{(l)}(z)$  referring to the disjoint vocabularies at each level, where  $i = 1, \dots, d$  and the span lengths  $\lambda$  range between the minimal ( $2^{L-l}$ ) and maximal ( $3^{L-l}$ ) value at this level. The  $L$ -th level tensor, for the sentence  $x_1, \dots, x_d$ , is initialized as  $M_{i,\lambda}^{(L)}(z) = \delta_{x_i, z}$ . Tensors at other levels are then obtained recursively, as recalled in App. B. Running this algorithm on a sentence  $x$ , one obtains  $Pr(x|\alpha) = M_{i,d}^{(0)}(\alpha)$  and the class entropy, which we average over both sentences and grammar realizations  $\mathbb{E}_{x,G}[H_L(\alpha|x)]$ . Fig. 3 displays this quantity as  $f$  is varied. Remarkably, ambiguity decreases rapidly at small  $f$  for larger  $L$ ; while at large  $f$  the entropy is maximal—indicating that classification is impossible beyond chance.

**Crossover point  $f_c$ .** We already noted that the number of trees grows exponentially as  $N_t \sim 2^{(\langle s \rangle^L - 1)/(\langle s \rangle - 1)}$ . As shown in App. A, the fraction  $F(d, L)$  of grammatical data (out of the total  $v^d$  which could be formed) given a typical parse tree at depth  $L$  decays exponentially as  $\sim f^{(\langle s \rangle^L - 1)/(\langle s \rangle - 1)}$ , where we recall  $f < 1$ . Naively, one expects a transition at  $FN_t \sim 1$  or  $f_c = 1/2$ : below  $f_c$ , the probability of finding two or more grammatical parse trees for the same sentence vanishes for large  $L$ , whereas for  $f > f_c$  this probability approaches one. This argument is mean-field in character and neglects correlations. An improved approximation for the characteristic crossover

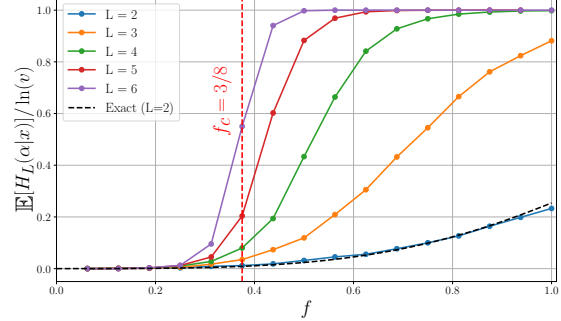


Figure 3. Crossover from local to global ambiguity as the fraction  $f$  of grammatical rules is tuned. Shown is the expected class entropy given a sentence  $\mathbb{E}[H_L(\alpha|x)]$  (normalized by  $\ln(v)$ ), which we compute numerically by running the parallelized inside algorithm and averaging over both sentences and grammar realizations. Red dashed lines indicate the theoretical estimate  $f_c = 3/8$  (App. B), while black dashed lines show  $\mathbb{E}[H_{L=2}(\alpha|x)]$ , which can be computed exactly (App. A).

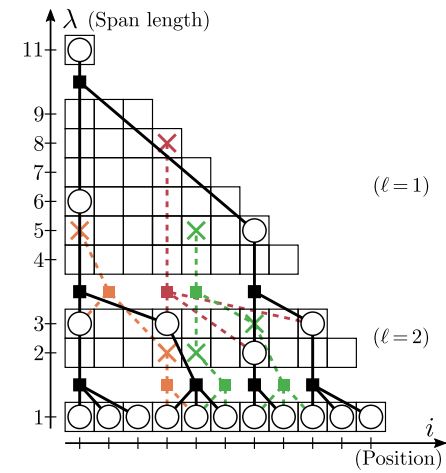


Figure 4. Illustration of the *inside algorithm* and the appearance of *spurious nonterminals*. Depicted are the inside tensors  $M_{i,\lambda}^{(l)}(z)$  created while parsing a sentence of length  $d=11$  and depth  $L=3$ . The third axis corresponding to nonterminals is not shown explicitly; instead we only distinguish between nonterminals belonging to the true parse tree (circles) and spurious ones (crosses). Spurious candidates can be built from purely spurious/true nonterminals in the level below (green/purple) or from a mixture (orange).

scale  $f_c$  can be obtained instead by studying the role of *spurious nonterminals*, as illustrated in Fig. 4. These are nonterminals built by the inside algorithm (due to syntactic ambiguity) which *do not* belong to the original parse tree which derived the sentence. Global ambiguity is determined by whether such spurious nonterminals can propagate all the way up to the root label. App. B estimates how the average number of candidate nonterminals built by the inside algorithm evolves with  $\ell$ , leading to a bifurcation in the large- $L$  limit for  $f_c = 3/8$ , in qualitative agreement with Fig. 3.

In this work, our main objective is to understand the sam-

ple complexity of the root classification task in the regime  $f < f_c$  where the grammar is globally unambiguous, and hence representative of natural language (which has evolved to allow efficient communication (Hahn et al., 2020)). The probability of multiple class labels given a sentence is then negligible. Boolean inside tensors  $N_{i,\lambda}^{(L)}(z)$  corresponding to  $\mathbf{1}\{Pr(x_i \dots x_{i+\lambda-1}|z) > 0\}$  indicating whether a nonterminal *can* yield the substring then suffice. It corresponds to the classic CYK (Cocke–Younger–Kasami) algorithm (Younger, 1967) used to identify if a sentence belongs to a language, which can be used to identify the unique class label  $\alpha$  of sentence  $x$ . We now provide a learning algorithm to model how deep nets can learn the CYK.

## 4. Learning Algorithm and Sample Complexity

Even in the globally unambiguous phase, local ambiguity hinders inference of the grammar rules: (A) the spans of the nonterminals are unknown, i.e. we don't know if a given pair/triple of tokens is generated by a single nonterminal; (B) some rules overlap, i.e. some pairs of tokens  $(a, b)$  can correspond either to a valid binary sibling pair or to a subsequence of a valid triple of ternary siblings  $(a, b, c)$  or  $(c, a, b)$ . In this section, we introduce an *iterative learning algorithm* that solves both problems, thus learning the root-classification task from data. The algorithm is based on a *method of moments* that we use here to infer the grammar's production rules level by level. The corresponding sample complexity is only polynomial in the typical sentence size as  $L$  increases, despite the exponentially growing number of parse tree topologies, each generating exponentially many distinct sentences. We will later argue that deep neural networks learn via a similar algorithm, and show empirically that they indeed enjoy the same sample complexity as our iterative learning algorithm.

**Assumptions:** The learning algorithm is given samples of ordered sentences  $\mathbf{X} = (X_1, \dots, X_d)$  from the RHM with variable arity, in the *asymptotic vocabulary size limit*

$$v \rightarrow \infty, \quad \text{with} \quad m_s = f_s v^{s-1} \quad \text{for} \quad s = 2, 3, \quad (1)$$

and in the *globally unambiguous phase*  $f_2, f_3 < f_c$ . The algorithm can store the position of each token. Furthermore, it assumes that the grammar consists of only binary and ternary production rules.

**The learning algorithm** consists of the following steps.

**Step 1:** (root-to-tokens covariances) Estimate the covariances between the root and pairs/triples of adjacent input

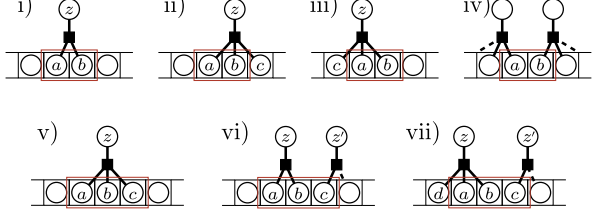


Figure 5. Decomposition of root-to-pair and root-to-triple covariances by the law of total covariance according to the local topology. Diagrams i) to iv) contribute to the root-to-pair covariance, while diagrams v), vi) and vii) to the root-to-triple one.

tokens,

$$C_2^{(L)} := \text{Cov} \left[ (X_I, X_{I+1}), X^{(0)} \right], \quad (2)$$

$$C_3^{(L)} := \text{Cov} \left[ (X_I, X_{I+1}, X_{I+2}), X^{(0)} \right], \quad (3)$$

where the average includes the position  $I$ .  $C_2$  is a  $v \times v \times v$  tensor,  $C_3$  is  $v \times v \times v \times v$ .

**Step 2:** (binary rules) For each pair  $(a, b)$  take the  $v$ -dimensional slice  $C_2((a, b), :)$ . The corresponding unit vectors cluster into  $v$  groups, one per level- $(L-1)$  nonterminal. These clusters consist of all the pairs  $(a, b)$  produced by the same nonterminal  $z$  via a binary rule, allowing one to reconstruct the latter. All the pairs that are not valid binary siblings have vanishing correlations for large  $v$  and can be discarded on that basis (details in subsection 4.1).

**Step 3:** (ternary rules) For each triple  $(a, b, c)$  define the  $v$ -dimensional vector  $C_3((a, b, c), :) - v^{-1}C_2((a, b), :) - v^{-1}C_2((b, c), :)$ . The corresponding unit vector cluster again into  $v+1$  groups: one for each nonterminal  $z = 1, \dots, v$  plus one for the triples that are not valid ternary siblings ( subsection 4.2).

**Step 4:** (candidate nonterminals) Use the level- $L$  rules inferred in steps 2 and 3 to define for each sentence nonterminal detectors,  $N_{i,s}^{(L-1)}(a) = 1$  if the terminals from  $i$  to  $i+s-1$  can be produced by nonterminal  $a$  and 0 otherwise. Multiplying detectors gives indicator functions of pairs and triples of level- $(L-1)$  nonterminals,

$$N_{i,s,s'}^{(L-1)}(a, b) = N_{i,s}^{(L-1)}(a)N_{i+s,s'}^{(L-1)}(b), \quad (4)$$

and  $N_{i,s,s',s''}^{(L-1)}(a, b, c)$  defined analogously for triples.

**Step 5:** (iterate) The covariances estimated from the full training set between pair/triple indicators and the root generalize Eq. 2 and Eq. 3 to level- $(L-1)$  nonterminals. Use  $C_2^{(L-1)}$  and  $C_3^{(L-1)}$  as in steps 2 and 3 to infer level- $(L-1)$  rules ( subsection 4.3), then apply the rules as in step 4 to build candidate level- $(L-2)$  nonterminals and pairs/triples thereof. Repeat until the root (level-0 nonterminal).

Once the rules are learned, they can be used to parse any sentence  $x$  and obtain the associated tree of nonterminal variables, including the root, as in the CYK algorithm.

#### 4.1. Root-to-pair covariance determines binary rules

The effect of local ambiguity on the statistics of pairs of adjacent tokens  $(X_I, X_{I+1})$  is illustrated in Fig. 5: the tokens can be binary siblings (probability  $p_{\text{bin}}$ ), but also part of a triple of ternary siblings  $(X_{I-1}, X_I, X_{I+1})$  or  $(X_I, X_{I+1}, X_{I+2})$  (probability  $p_{\text{ter}}$  each), or sit across the boundary between two spans (probability  $p_{\text{cross}}$ ). The root-to-pair covariance from Eq. 2 takes contributions from all these cases, as is evident from a linear decomposition based on the law of total covariance, also illustrated in Fig. 5 (diagrams i) to iv), see subsection C.2 for details)). Nevertheless, in the limit Eq. 1, the asymptotic behavior of  $C_2^{(L)}$  is dominated by the contribution of binary siblings (diagram i)). Namely, as proved in subsection C.2,

$$C_2^{(L)}((a, b), \alpha) \approx p_{\text{bin}} \sum_{z=1}^v R_{z \rightarrow (a, b)}^{(L)} C_1^{(L-1)}(z, \alpha), \quad (5)$$

where  $R_{z \rightarrow (a, b)}^{(L)}$  denotes the probability of the level- $L$  production rule  $z \rightarrow (a, b)$  and  $C_1^{(L-1)}$  the root-to-nonterminal covariance matrix. Since  $R_{z \rightarrow (a, b)}^{(L)}$  selects the only  $z$  that produces  $(a, b)$  as binary siblings, all the pairs  $(a, b)$  produced by the same nonterminal  $z$  have  $C_2^{(L)}((a, b), \alpha)$  proportional to  $C_1^{(L-1)}(z, \alpha)$ . As a result, the directions of the  $v$ -dimensional slices  $C_2^{(L)}((a, b), :)$  cluster by the generating nonterminal  $z$ , as illustrated in Fig. 6, panel a. The set of pairs  $(a, b)$  belonging to the same cluster coincides with the set of binary rules emanating from the same nonterminal.

#### 4.2. Whitened root-to-triple covariance determines ternary rules

The root-to-triple covariance is also affected by the same sources of ambiguity as  $C_2^{(L)}$ , as illustrated in Fig. 5 (diagrams v), vi) and vii)). In addition, even in the asymptotic limit, the contribution of ternary siblings (diagram v))competes with those where two of the three tokens form a pair of binary siblings (vi) and vii)). This competition prevents the direct inference of ternary rules from  $C_3^{(L)}$ , as highlighted in Fig. 6, panel b. However, as proved in subsection C.3, the spurious binary contributions converge to a simple correction of the root-to-pair covariance,

$$\begin{aligned} C_3^{(L)}((a, b, c), \alpha) &\approx p_{\text{ter}} \sum_{z=1}^v R_{z \rightarrow (a, b, c)}^{(L)} C_1^{(L-1)}(z, \alpha) + \\ &\quad \frac{1}{v} \left( C_2^{(L)}((a, b), \alpha) + C_2^{(L)}((b, c), \alpha) \right). \end{aligned} \quad (6)$$

The binary contributions are thus easily removed, and the clustering property restored, as shown in Fig. 6, panel c.

#### 4.3. Candidate nonterminals and covariance with the root

Having identified the level- $L$  rules, we can build a detector for candidate nonterminals,  $N_{i,s}^{(L-1)}(a) = 1$  if the terminals  $(X_i, \dots, X_{i+(s-1)})$  can be produced by nonterminal  $a$ , and 0 otherwise. Pair and triple detectors can also be built by checking, for each  $N_{i,s}^{(L-1)}(a) = 1$ , if there is some  $b$  and  $s'$  such that  $N_{i+s,s'}^{(L-1)}(b) = 1$  (thus a valid pair  $(a, b)$ ), and some  $c$  and  $s''$  such that  $N_{i+s+s',s''}^{(L-1)}(c) = 1$  (thus a valid triple  $(a, b, c)$ ). Notice, however, that not all candidates correspond to true nonterminals, as there is a probability  $\approx f$  that a sequence of adjacent terminals that are *not* binary/ternary siblings is compatible with some rule—we refer to these cases as *spurious*. All indicators introduced can be expressed as the sum of a true and a spurious indicator.

Consequently, the covariances between the root and pairs or triples of candidate nonterminals decompose into true and spurious contributions. The true term is analogous to those analyzed in subsection 4.1 and subsection 4.2. The spurious term, instead, takes contributions from all the possible local configurations (including topology and nonterminal values) of parse trees that produce the same ambiguous local sequence of terminals. Nevertheless, the true term dominates the covariances in the asymptotic vocabulary size limit, allowing for the iteration of the inference steps of subsection 4.1 and subsection 4.2.

While we defer the proof to subsection C.4, the idea is simple. First, we can use the law of total covariance again to express the spurious covariance as a weighted sum of terms corresponding to all the possible local topologies  $t$  and non-terminal values  $X_t^{(L-1)}$  that produce the same ambiguous local sequence. As a result, the spurious term is the average of root-to-level- $(L-1)$  covariances with different, unrelated sets of symbols. Since these covariances are almost uncorrelated, the average results in a reduction of scale of the order of the inverse square root of the number of terms appearing in the average. As long as the probability  $\approx f$  that a sequence of adjacent terminals that are *not* binary/ternary siblings is compatible with some rule is finite, the number of such terms scales at least as  $v$  in the asymptotic limit. Hence, the spurious term vanishes in the asymptotic limit.

#### 4.4. Sample Complexity

The sample complexity of our iterative learning algorithm is determined by the estimation of all the covariances involved. As proved in subsection C.5, all root-to-pair and root-to-triple covariances have a well-defined typical scale in the asymptotic limit Eq. 1, given by the standard deviation of the

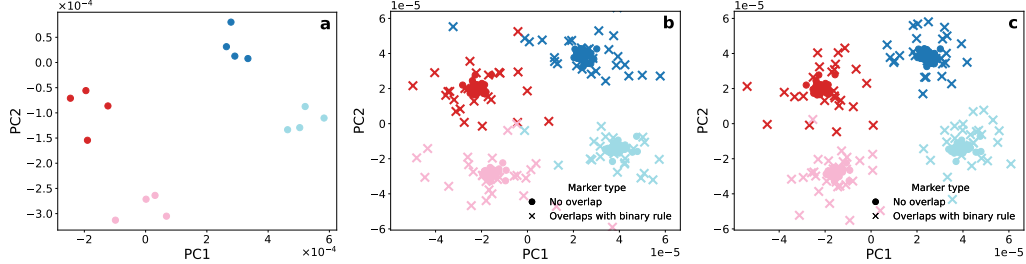


Figure 6. Illustration of several steps of the algorithm with parameters  $v = 16$ ,  $f = 1/4$  ( $m_2 = 4$ ,  $m_3 = 64$ ) and  $L = 2$ . **a** corresponds to step 2, that builds the first level of latent variables by clustering root-to-pair correlation vectors (here projected on two dimensions with PCA) from a finite training set of  $P = 8 \times 10^6$  sentences. For visualization purposes, we show only 4 out of  $v$  clusters in all panels; different nonterminals correspond to different colors. **b** highlights that ternary rules that overlap with some grammatical binary rule (denoted by crosses, contrasted with nonoverlapping ternary rules denoted by dots) do not cluster. **c** corresponds to step 3: it removes the binary contribution from the root-to-triple correlations, showing how the clusters become cleanly separated (it becomes perfect for  $v \rightarrow \infty$ ).

Frobenius norm over realizations of the generative model. In particular,

$$\begin{aligned} \|C_2^{(\ell)}\|_F &= O\left(\sqrt{\frac{(p_2^2/2)^{\ell-1}}{vm_2^\ell}}\right), \\ \|C_3^{(\ell)}\|_F &= O\left(\sqrt{\frac{(p_2^2/2)^{\ell-1}}{vm_3m_2^{\ell-1}}}\right). \end{aligned} \quad (7)$$

Note that these scales correspond to reducing correlations by a factor of  $\sqrt{m_s}$  for each  $s$ -ary production rule traversed when connecting the desired level- $\ell$  pair or triple to the root. Then, since  $m_3 > m_2$  in the regime described by Eq. 1, the dominant scale corresponds to the *easiest branch*, where the number of ternary rules is minimal.

The covariance with the smallest scale— $C_3^{(L)}$ —is the hardest to measure, hence it controls the sample complexity. Using a standard decomposition of the empirical covariances into population limit plus sampling noise, then controlling the sampling noise with the inverse square root of the number of samples  $P$  (details in subsection C.5) gives  $P^* = O(\|C_3^{(L)}\|_F^{-2})$ , i.e.:

$$P^* = O((p_2^2/2)^{1-L}vm_3m_2^{L-1}) \quad (8)$$

## 5. Empirical measurements of $P^*$

The learning algorithm we proposed is inspired by CNNs: (i) for the first iteration at least, the clustering based on correlations can be achieved with one step of gradient descent (Malach & Shalev-Shwartz, 2018; Cagnetta et al., 2024) and (ii) acting on the correlation between substrings and task across the entire sentence is automatic with weight sharing. We thus first test our predictions on sample complexity in CNNs, before showing that they hold more generally, including in transformers.

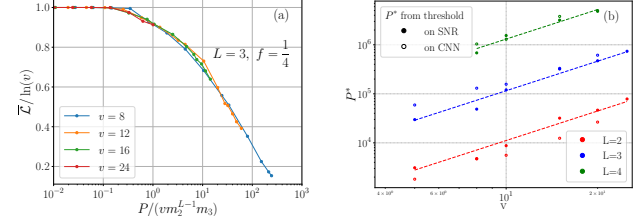


Figure 7. (a) Additional empirical tests of the sample complexity prediction (8) in CNNs. CNN test loss  $\bar{L}$  (normalized by random guessing), averaged over grammar, data, and network realizations, vs. the number of training samples  $P$ , for  $L=3$ , fixed  $f=1/4$  and increasing  $v$ . We find a good collapse confirming the scaling  $P^* \sim v^5$ . (b) Sample complexity prediction obtained by thresholding the inverse SNR computed from joint triple–root statistics (see App. E), compared to the empirical value extracted from Fig. 1(a), finding excellent agreement.

## 5.1. Tests on CNNs

We consider hierarchical CNNs of depth  $L$ , with filters of size 4 and stride 2 such that both rule types are covered (see App. D). These are trained by standard SGD on the classification cross-entropy loss, using  $P$  training points  $(x, \alpha(x))$  from our varying tree dataset.

**$P^*$  v.s. vocabulary and rule numbers:** We test the dependence of Eq. 8 on  $v, m_2, m_3$  in two ways. (i) We set  $f=1/v$  and vary  $v$  so that  $P^* \sim v m_2^{L-1} m_3 \sim v^2$ . Fig. 1.(a) shows the raw learning curves. Rescaling the training set size  $P$  by the predicted  $P^*$  leads to a remarkable *collapse* shown in Fig. 1.(b), confirming the theory. (ii) Next, we increase  $v$  with fixed  $f=1/4 < f_c$ . For  $L=3$ , Eq. 8 then leads to  $P^* \sim v^5$ . Again, the excellent collapse displayed in Fig. 7.(a) validates our prediction.

**$P^*$  v.s. depth  $L$ :** As computed in Sec. 4, the key triple-root correlation required for learning is dominated by the “easy branches” with binary productions except for the final level- $L$  production. As  $L$  increases, these branches occur with a

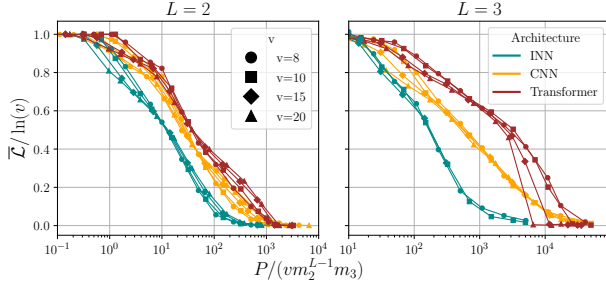


Figure 8. Average normalized test loss  $\bar{\mathcal{L}}$  vs. rescaled training samples  $P$ , comparing the sample efficiency of the INN, CNN and transformer for  $L=2$  and  $L=3$ . We consider the setting of Fig. 7(a), of increasing  $v$  with  $f=1/v$ , so that  $P^* \sim v m_2^{L-1} m_3 \sim v^2$ , a scaling which is found to be consistent with all three architectures.

smaller probability, leading to a factor  $(p_2^2/2)^{1-L}$  in Eq. 8. To test this prediction, we (i) extract  $P^*(v, L)$  from the learning curves in Fig. 1.(a) by setting a threshold and (ii) measure empirically a signal-to-noise ratio corresponding to the measurement of the joint triple-root statistics (see App. E for details). Fig. 7.(b) shows that this quantity tracks accurately the sample complexity as predicted, and both quantities follow the expected quadratic dependence on  $v$ .

## 5.2. Other architectures

We now consider (a) a vanilla encoder-only transformer (see App. D for details), and (b) an alternative hierarchical convolutional network, which we refer to as Inside Neural Network (INN). Unlike the transformer, the INN is finetuned to our task: it uses a separate binary and ternary filter at each layer, and builds hidden representations mirroring the inside tensors  $M_{i,\lambda}^{(l)}$  (Fig. 4) by stacking convolutions for each span length (see App. D).

Fig. 8(a,b) displays training curves for  $L=2$  and  $L=3$  respectively. In both cases, sample size was rescaled by our prediction for  $P^*$ , and shows an excellent collapse for all architectures considered- illustrating the broad applicability of our theory. Although sample complexity scales similarly in all architectures, in terms of pre-factors the INN performs better than the transformers, while the CNN is intermediary; as expected with respect to the inductive bias of these architectures.

## 6. Conclusion

We have provided a theory for how deep nets learn to parse based on local correlations, leading to a prediction for sample complexity confirmed in a variety of architectures. This approach can explain how the representation of abstract semantic notions invariant to syntactic details of the sentence - modeled here as latent variables that can generate many possible visible substrings - can be learned in deep nets.

Note that although we have focused on a supervised task for concision of presentation, following (Cagnetta & Wyart, 2024; Cagnetta et al., 2025) we expect our results to readily apply to next-token prediction. In that case, the key signals are the correlation between the last token and pairs or triples of tokens further away in the sentence. As the training set-size increases, longer-range correlations can be resolved, and latent variables of higher level  $L - \ell$  can be constructed. For regular trees with single branching ratio and  $m$  production rules per latent, it led to a sample complexity to construct latent variables at level  $\ell$  that followed  $P_\ell \sim vm^{2(L-\ell)+1}$  (Cagnetta & Wyart, 2024). Following our result that correlations are dominated by the easiest branch, we expect that the sample complexity for varying trees generalizes to  $P_\ell \sim vm_2^{2(L-\ell)}m_3$ .

Our theory of learning is based on a proposed algorithm, and not on a mathematical description of gradient descent (GD) that is well beyond the state of the field for deep architectures. That said, our approach puts forward certain mechanisms at play during training, and it would be interesting to establish how they can be realized with GD. That includes: (i) the disambiguating step of the algorithm that clusters triplet strings together after removing the signal of spurious pairs. Although it is well-known that clustering based on correlations can be achieved with one GD step (Malah & Shalev-Shwartz, 2018; Cagnetta et al., 2024), the possibility that the new procedure may be achievable in a few steps of GD is an interesting question for the future. (ii) Maintaining track of the spans of latent variables, and building strings of adjacent ones (as needed to iterate our learning algorithm across depth). On this front, the question of how CNNs build adjacency from their internal representations is less clear. We expect that again, clustering by correlation is at play, since non-adjacent strings of latent variables will display very weak correlations with the task in comparison to adjacent ones.

## Limitations

One limitation is that we have considered grammars of uniform depth. Important works for the future include extending these results to (i) syntax where some production rules can be used recursively, leading to non-uniform depth (Schulz et al., 2025) and (ii) more structured syntax such as attribute (Knuth, 1968) or dependency grammars that LLMs encode in intriguing ways (Diego-Simón et al., 2024).

## Acknowledgments

The calculations have been performed using the facilities of the Scientific IT and Application Support Center of EPFL. The work of FC was supported by the European Union’s Horizon Europe program under the Marie Skłodowska-

Curie grant agreement No. 101154584. This work was supported by the Simons Foundation through the Simons Collaboration on the Physics of Learning and Neural Computation (Award ID: SFI-MPS-POL00012574-05), PI Wyart.

## References

Allen-Zhu, Z. and Li, Y. Physics of Language Models: Part 1, learning hierarchical language structures. *Transactions on Machine Learning Research*, 2025. URL <https://openreview.net/forum?id=mPQKyzkA1K>.

Bailly, R., Carreras, X., Luque, F. M., and Quattoni, A. Unsupervised spectral learning of WCFG as low-rank matrix completion. In *Proceedings of the 2013 Conference on Empirical Methods in Natural Language Processing*, pp. 624–635, Seattle, Washington, USA, 2013. Association for Computational Linguistics. doi: 10.18653/v1/D13-1059. URL <https://aclanthology.org/D13-1059>.

Baker, J. K. Trainable grammars for speech recognition. *The Journal of the Acoustical Society of America*, 65: S132, 1979. ISSN 0001-4966. doi: 10.1121/1.2017061. URL <https://doi.org/10.1121/1.2017061>.

Balle, B., Hamilton, W., and Pineau, J. Methods of moments for learning stochastic languages: Unified presentation and empirical comparison. In *Proceedings of the 31st International Conference on Machine Learning*, pp. 1386–1394. PMLR, 2014. URL <https://proceedings.mlr.press/v32/balle14.html>. ISSN: 1938-7228.

Cagnetta, F. and Wyart, M. Towards a theory of how the structure of language is acquired by deep neural networks. In *Advances in Neural Information Processing Systems*. Neural Information Processing Systems Foundation, Inc., 2024. doi: 10.52202/079017-2645. URL [https://proceedings.neurips.cc/paper\\_files/paper/2024/hash/9740da1c07c7b451af14e11523f95271-Abstract.html](https://proceedings.neurips.cc/paper_files/paper/2024/hash/9740da1c07c7b451af14e11523f95271-Abstract.html).

Cagnetta, F., Petrini, L., Tomasini, U. M., Favero, A., and Wyart, M. How deep neural networks learn compositional data: The random hierarchy model. *Physical Review X*, 14(3):031001, 2024.

Cagnetta, F., Favero, A., Sclocchi, A., and Wyart, M. Scaling laws and representation learning in simple hierarchical languages: Transformers vs. convolutional architectures. *Physical Review E*, 112(6):065312, 2025. doi: 10.1103/PhysRevE.112.065312.

Chomsky, N. *Syntactic structures*. Syntactic structures. Mouton, Oxford, England, 1957. Pages: 116.

Chomsky, N. Rules and representations. *Behavioral and Brain Sciences*, 3(1):1–15, 1980. ISSN 1469-1825, 0140-525X. doi: 10.1017/S0140525X00001515. URL <https://www.cambridge.org/core/journals/behavioral-and-brain-sciences/article/rules-and-representations/BB96E4E09C461EFC230F72A9D7BDF603>.

Clark, A. Computational learning of syntax. *Annual Review of Linguistics*, 3(1):107–123, 2017. ISSN 2333-9683, 2333-9691. doi: 10.1146/annurev-linguistics-011516-034008. URL <https://www.annualreviews.org/doi/10.1146/annurev-linguistics-011516-034008>.

Clark, A. and Yoshinaka, R. Polynomial identification in the limit of substitutable context-free languages. *Journal of Machine Learning Research*, 14:303–325, 2013. URL <https://www.jmlr.org/papers/v14/clark13a.html>.

Cohen, S. B. and Smith, N. A. Empirical risk minimization for probabilistic grammars: Sample complexity and hardness of learning. *Computational Linguistics*, 38(3): 479–526, 2012.

DeGiuli, E. Random language model. *Physical Review Letters*, 122(12):128301, 2019.

Dempster, A. P., Laird, N. M., and Rubin, D. B. Maximum likelihood from incomplete data via the EM algorithm. *Journal of the Royal Statistical Society. Series B (Methodological)*, 39(1):1–38, 1977. ISSN 0035-9246. URL <https://www.jstor.org/stable/2984875>.

Devlin, J., Chang, M.-W., Lee, K., and Toutanova, K. Bert: Pre-training of deep bidirectional transformers for language understanding. In *North American Chapter of the Association for Computational Linguistics*, 2019. URL <https://api.semanticscholar.org/CorpusID:52967399>.

Diego-Simón, P. J., D’Ascoli, S., Chemla, E., Lakretz, Y., and King, J.-R. A polar coordinate system represents syntax in large language models. *Advances in Neural Information Processing Systems*, 37:105375–105396, 2024.

Ellis, N. C. Frequency effects in language processing: A review with implications for theories of implicit and explicit language acquisition. *Studies in second language acquisition*, 24(2):143–188, 2002.

Favero, A., Sclocchi, A., Cagnetta, F., Frossard, P., and Wyart, M. How compositional generalization and creativity improve as diffusion models are trained. In *Proceedings of the 42nd International Conference on Machine Learning*, volume 267 of *Proceedings of Machine Learning Research*, pp. 16286–16306. PMLR,

2025. URL <https://proceedings.mlr.press/v267/>. Poster Presentation.

Frazier, L. and Rayner, K. Making and correcting errors during sentence comprehension: Eye movements in the analysis of structurally ambiguous sentences. *Cognitive Psychology*, 14(2):178–210, 1982. ISSN 0010-0285. doi: 10.1016/0010-0285(82)90008-1.

Goodman, J. Parsing algorithms and metrics. In *34th Annual Meeting of the Association for Computational Linguistics*, pp. 177–183, Santa Cruz, California, USA, 1996. Association for Computational Linguistics. doi: 10.3115/981863.981887. URL <https://aclanthology.org/P96-1024>.

Gurnee, W., Ameisen, E., Kauvar, I., Tarn, J., Pearce, A., Olah, C., and Batson, J. When models manipulate manifolds: The geometry of a counting task, 2026. URL <https://arxiv.org/abs/2601.04480>. arXiv:2601.04480.

Hahn, M., Jurafsky, D., and Futrell, R. Universals of word order reflect optimization of grammars for efficient communication. *Proceedings of the National Academy of Sciences*, 117(5):2347–2353, 2020.

Hsu, D., Kakade, S. M., and Liang, P. Identifiability and unmixing of latent parse trees. In *Advances in Neural Information Processing Systems 25*. Neural Information Processing Systems Foundation, Inc., 2012. URL [https://proceedings.neurips.cc/paper\\_files/paper/2012/file/50c3d7614917b24303ee6a220679dab3-Paper.pdf](https://proceedings.neurips.cc/paper_files/paper/2012/file/50c3d7614917b24303ee6a220679dab3-Paper.pdf).

Jerad, S., Svet, A., Hao, S., Cotterell, R., and Merrill, W. Context-free recognition with transformers, 2026. URL <https://arxiv.org/abs/2601.01754>. arXiv:2601.01754.

Klein, D. and Manning, C. Corpus-based induction of syntactic structure: Models of dependency and constituency. In *Proceedings of the 42nd Annual Meeting of the Association for Computational Linguistics (ACL-04)*, pp. 478–485, Barcelona, Spain, 2004. doi: 10.3115/1218955.1219016. URL <https://aclanthology.org/P04-1061/>.

Knuth, D. E. Semantics of context-free languages. *Mathematical systems theory*, 2(2):127–145, 1968.

Malach, E. and Shalev-Shwartz, S. A provably correct algorithm for deep learning that actually works, 2018. URL <https://arxiv.org/abs/1803.09522>. arXiv:1803.09522.

Manning, C. D., Clark, K., Hewitt, J., Khandelwal, U., and Levy, O. Emergent linguistic structure in artificial neural networks trained by self-supervision. *Proceedings of the National Academy of Sciences*, 117(48):30046–30054, 2020.

Mossel, E. Deep learning and hierarchical generative models, 2016. URL <https://arxiv.org/abs/1612.09057>. arXiv:1612.09057.

Pereira, F. and Schabes, Y. Inside-outside reestimation from partially bracketed corpora. In *30th Annual Meeting of the Association for Computational Linguistics*, pp. 128–135, Newark, Delaware, USA, 1992. Association for Computational Linguistics. doi: 10.3115/981967.981984. URL <https://aclanthology.org/P92-1017/>.

Peters, M. E., Neumann, M., Zettlemoyer, L., and Yih, W. Dissecting contextual word embeddings: Architecture and representation. In Riloff, E., Chiang, D., Hockenmaier, J., and Tsujii, J. (eds.), *Proceedings of the 2018 Conference on Empirical Methods in Natural Language Processing*, pp. 1499–1509, Brussels, Belgium, 2018. Association for Computational Linguistics. doi: 10.18653/v1/D18-1179. URL <https://aclanthology.org/D18-1179>.

Radford, A., Narasimhan, K., Salimans, T., and Sutskever, I. Improving language understanding with unsupervised learning, 2018. URL <https://openai.com/research/language-unsupervised>. Technical report, OpenAI.

Saffran, J. R. and Kirkham, N. Z. Infant statistical learning. *Annual Review of Psychology*, 69:181–203, 2018.

Saffran, J. R., Aslin, R. N., and Newport, E. L. Statistical learning by 8-month-old infants. *Science*, 274(5294):1926–1928, 1996.

Schulz, L. Y., Mitropolsky, D., and Poggio, T. Unraveling syntax: How language models learn context-free grammars, 2025. URL <https://arxiv.org/abs/2510.02524>. arXiv:2510.02524.

Templeton, A., Conerly, T., Marcus, J., Lindsey, J., Bricken, T., Chen, B., Pearce, A., Citro, C., Ameisen, E., Jones, A., Cunningham, H., Turner, N. L., McDougall, C., MacDiarmid, M., Freeman, C. D., Sumers, T. R., Rees, E., Batson, J., Jermyn, A., Carter, S., Olah, C., and Henighan, T. Scaling monosematicity: Extracting interpretable features from claude 3 sonnet. <https://transformer-circuits.pub/2024/scaling-monosematicity/index.html>, 2024.

Tenney, I., Das, D., and Pavlick, E. BERT rediscovers the classical NLP pipeline. In Korhonen, A., Traum, D., and Màrquez, L. (eds.), *Proceedings of the 57th Annual Meeting of the Association for Computational Linguistics*, pp. 4593–4601, Florence, Italy, 2019. Association for Computational Linguistics. doi: 10.18653/v1/P19-1452. URL <https://aclanthology.org/P19-1452>.

Vaswani, A., Shazeer, N., Parmar, N., Uszkoreit, J., Jones, L., Gomez, A. N., Kaiser, L., and Polosukhin, I. Attention is all you need. In *Advances in Neural Information Processing Systems*, volume 30, 2017.

Yang, G. and Hu, E. J. Tensor programs iv: Feature learning in infinite-width neural networks. In *Proceedings of the 38th International Conference on Machine Learning*, volume 139 of *Proceedings of Machine Learning Research*, pp. 11773–11783. PMLR, 2021. URL <https://proceedings.mlr.press/v139/yang21c.html>.

Younger, D. H. Recognition and parsing of context-free languages in time  $n^3$ . *Information and Control*, 10(2): 189–208, 1967.

Zhao, H., Panigrahi, A., Ge, R., and Arora, S. Do transformers parse while predicting the masked word? In Bouamor, H., Pino, J., and Bali, K. (eds.), *Proceedings of the 2023 Conference on Empirical Methods in Natural Language Processing*, pp. 16513–16542, Singapore, 2023. Association for Computational Linguistics. doi: 10.18653/v1/2023.emnlp-main.1029. URL <https://aclanthology.org/2023.emnlp-main.1029/>.

## A. Model Properties: top-down master equations

We give here additional details of our synthetic grammar, starting with the distribution of sentence lengths.

### A.1. Distribution of sentence lengths

We denote the distribution of sentence lengths  $d$  at depth  $L$  by  $P(d, L)$ . This follows the following top-down master equation, initialized at  $P(d, L=0) = \delta_{d,1}$ :

$$P(d, L+1) = \sum_{d'=\lceil d/3 \rceil}^{\lfloor d/2 \rfloor} \frac{d'!}{(3d'-d)!(d-2d')!} \left(\frac{1}{2}\right)^{d'} P(d', L) \quad (9)$$

where the combinatorial factor accounts for the number of ways of choosing binary/ternary branchings for the sequence of  $d'$  parent nodes given the target length  $d$ , and the  $1/2$  reflects equally probable branchings.

To understand how the fluctuations of this multiplicative process scale, we can reason as follows. The sentence length at the next depth  $L+1$  is given by the product  $d_{L+1} = r_L \times d_L$ , so that, at depth  $L$ ,  $\log(d_L) = \sum_{L'=0}^{L-1} \log(r_{L'})$ . Here,  $r_L$  is a random variable, which will clearly have mean  $\langle r_L \rangle = 2.5$ . In general, its value will be set by a weighted average of 2 and 3, where the weights correspond to the fraction of  $d_L$  symbols which give rise respectively to 2 and 3 descendants. That is

$$r_L = \frac{2n(r=2) + 3(d_L - n(r=2))}{d_L} \quad (10)$$

where  $n(r=2) \sim \text{Binom}(d_L, 1/2)$ . For large  $d_L$ , we can approximate this as a Gaussian  $n(r=2) \sim \mathcal{N}(d_L/2, d_L/4)$ .  $r_L$  is simply a linear combination of Gaussians, and one can therefore calculate its mean and variance.  $\langle r_L \rangle = 2.5$ , while  $\sigma_r^2 = 13/(4d_L)$ .

We may equivalently consider the evolution of the log-sentence lengths,  $\log(d_{L+1}) = \log(r_L) + \log(d_L)$ . The mean and variance of  $\log(r_L)$  can be estimated using the Delta method: the mean of  $\log(r_L)$  is  $\log(2.5)$  up to a  $1/d_L \sim 1/2.5^L$  correction, and, more importantly, its variance goes as  $13/(2.5^2 4d_L) \sim 1/d_L$ .

Therefore, for  $L > 3$  we can neglect the fluctuations of  $r_L$  around  $\log(2.5)$ , and the distribution is just translated by a fixed amount from one layer to the next (Fig. 9). Equivalently, in probability space (Fig. 10), we find convergence to a scaling function, once we rescale to  $(d - 2.5^L)/(2.5^L)$ . The shape of this fixed distribution remains practically identical beyond  $L = 3$ , which is in turn just a slightly smoothed version of the distribution at  $L = 2$ .

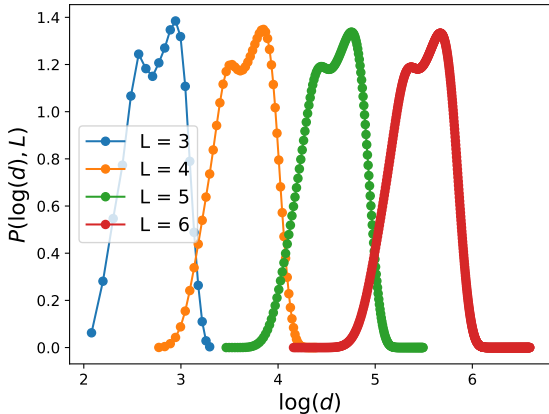


Figure 9. In log-space, the multiplicative process converges to a constant translation by  $\log(2.5)$  beyond  $L = 3$ .

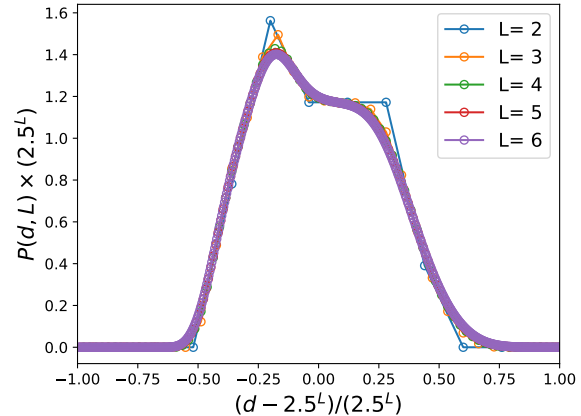


Figure 10. Scaling function in probability space. Asymptotically, this corresponds to a  $\times 2.5$  dilation of a fixed distribution (in practice this holds already for  $L > 3$ ).

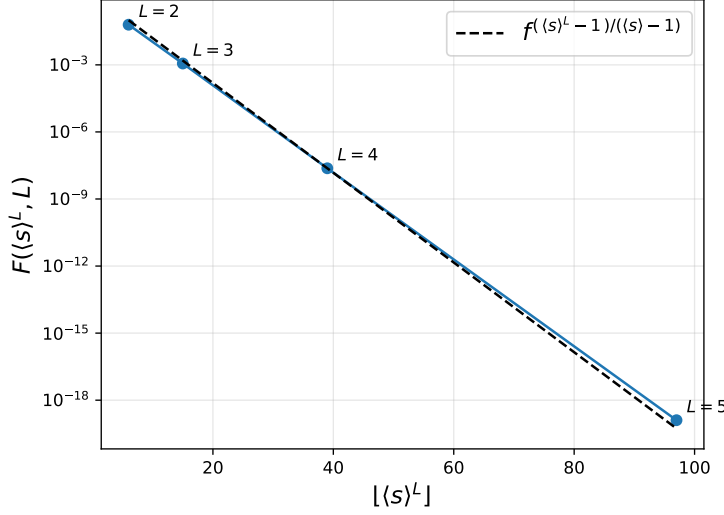


Figure 11. Numerical implementation of (Eq. 12) to obtain the fraction of grammatical data,  $F(d, L)$ , with  $f=1/2$  (the  $f < 1$  value can be chosen arbitrarily). Evaluating at the typical sentence length, we confirm the expected scaling  $\sim f^{((\langle s \rangle^L - 1)/(\langle s \rangle - 1))}$ .

## A.2. Number of tree topologies and fraction of grammatical data

We turn next to two additional important quantities, the number of topologically distinct trees for a sentence length  $d$  at depth  $L$ , and the fraction of generated data with respect to the total possible sentences. The master equation for the first reads

$$N_t(d, L+1) = \sum_{d'=\lceil d/3 \rceil}^{\lfloor d/2 \rfloor} \frac{d'!}{(3d'-d)!(d-2d')!} N_t(d', L) \quad (11)$$

initialized as  $N_t(d, L=1) = \delta_{d,2} + \delta_{d,3}$ . By applying Stirling's formula to the factorials, it is simple to show that this scales asymptotically as  $N_t(\langle s \rangle^L, L) \sim 2^{((\langle s \rangle^L - 1)/(\langle s \rangle - 1))}$ .

We turn next to the fraction  $F$  of grammatical sentences with respect to the total possible  $v^d$  given a tree topology, for a given sentence length  $d$  and depth  $L$ , averaged over the possible tree topologies compatible with  $(d, L)$ . It is easy to show that for a fixed topology (Cagnetta et al., 2024)), a factor  $f$  is accumulated for each branching made within the tree. With a fixed branching ratio  $s$ , this leads to the result that at depth  $L$ ,  $F = f^{((s^L - 1)/(s - 1))}$ , where  $(s^L - 1)/(s - 1)$  is the number of internal nodes of the tree. In the varying tree case, we are interested in the equivalent quantity, but which takes into account fluctuations of the tree topology once we fix a value  $(d, L)$ . This will be given by

$$F(d, L+1) = \frac{\sum_{d'=\lceil d/3 \rceil}^{\lfloor d/2 \rfloor} \frac{d'!}{(3d'-d)!(d-2d')!} \left(\frac{1}{2}\right)^{d'} f^{d'} F(d', L)}{\sum_{d'=2^L}^{3^L} \frac{d'!}{(3d'-d)!(d-2d')!} \left(\frac{1}{2}\right)^{d'}} \quad (12)$$

with  $F(d, L=1) = f(\delta_{d,2} + \delta_{d,3})$ . The meaning of this formula is to take the fraction  $F$  values at the previous layer for each  $d'$ , and multiply this by  $f^{d'}$  (recall that  $f$  must be raised to the number of branchings). Finally, this has to be weighed by the probability of having an incoming branching from  $(d', L)$ , leading to the normalization term in the denominator. We have shown in A.1 that after the first layers fluctuations around the multiplicative factor  $\langle s \rangle$  can be neglected: one therefore expects also here that, this fraction of data given a tree topology, scales, for typical sentences, asymptotically with the typical number of internal nodes as  $F(\langle s \rangle^L, L) \sim f^{((\langle s \rangle^L - 1)/(\langle s \rangle - 1))}$ . We confirm this in Fig. 11, where we implement numerically Eq. 12.

## A.3. Top-down approach to the class entropy

We present here a top-down derivation of the class entropy, which gives the exact prediction for  $L = 2$  shown in Fig. 3. For the expected class entropy  $\mathbb{E}_{x, \mathcal{G}}[H_L(\alpha|x)]$  given a sentence  $x$ , we can evaluate this by decomposing firstly into sentence

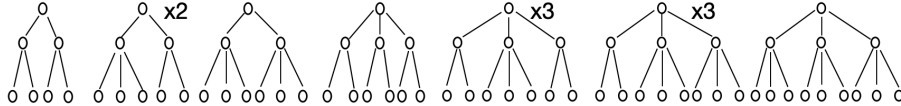


Figure 12. Sketch showing the 12 distinct tree topologies at  $L = 2$ . Note that for  $d = 5$  there are two permutations of the tree, and 3 permutations for  $d = 7, 8$ . The probability of each individual topology is simply given by  $p_2 = p_3 = 1/2$  raised to the number of branchings.

lengths

$$\mathbb{E}[H_L(\alpha|x)] = \sum_{d'} \mathbb{E}[H_L(\alpha|x; d')] P(d', L) \quad (13)$$

For  $L = 2$ , one can then derive the expression (shown in Fig. 3 of the main text)

$$\mathbb{E}[H_2(\alpha|x)](f) = \frac{1}{4} f^3 H(1/2, 1/2) + \frac{3}{16} \left( \frac{2}{3} f^3 + \frac{1}{3} f^4 \right) H(1/3, 2/3) + \frac{3}{8} (2f^4(1-f^4) H(1/2, 1/2) + f^8 H(1/3, 1/3, 1/3)) \quad (14)$$

where we use the notation  $H(\{p_i\}) = -\sum_i p_i \ln(p_i)$ . For each value of  $d' = 4, \dots, 9$  we use the value of  $F(d', L=2)$  as the probability of success of finding an additional parse tree deriving the sentence, among the  $N_t(d, L=2) - 1$  possible topologies (the 12 topologies at  $L = 2$  are sketched in Fig. 12), weighing this by the probability  $P(d', L)$ . If an additional tree is found, the entropy is then given by the set of probabilities  $\{p_i\}$  of the topologies. For  $d = 7, 8$  (last term), there are  $N_t = 3$  topologies, so that either one more or two more can be found. Note furthermore that for  $d = 6$  (second term), the 2–2–2 topology is a factor 2 less probable than the 3–3 topology, due to the extra branching. Eq. 14 is valid for  $v \gg 1$ , as we have assumed that each additional parse tree corresponds to a different label; accounting for coinciding labels leads to corrections of  $\mathcal{O}(1/v)$ .

As mentioned in the main text, extending the reasoning behind (14) to deeper grammars,  $L > 2$ , fails, for the following reason. In deriving (14) we implicitly make an independence assumption, namely that the probability of finding an additional parse tree is independent of the ground truth (or planted) tree. As discussed in the main text (see e.g. Fig. 4), however, spurious latents can be formed from latents on the ground truth tree, so that the later acts as an additional source leading potentially to additional parse trees. The reason (14) nonetheless holds for  $L = 2$  are geometric constraints for forming a full span: for  $L = 2$ , additional class labels can only be built using purely spurious latents at level-1. For example for  $d = 5$ , where there are two possible topologies 3–2 or 2–3, if the ground truth is 3–2 and a spurious latent is generated for the pair at the start of the sentence, this spurious latent cannot build a complete span together with the original true latent of the second pair, as this would only sum up to a total span length of 4.

## B. Inside algorithm and bottom-up transition theory

### B.1. Tensorial form of the inside algorithm

We provide here firstly the full form of the tensorial, layered inside algorithm. We recall that the token-level inside tensor for each sentence is initialized as  $M_{i,\lambda}^{(L)}(z) = \delta_{x_i, z}$ . To build layer by layer the tensors at other levels, we follow

$$\begin{aligned} M_{i,\lambda}^{(l-1)}(z) &= \sum_{a,b=1}^v \sum_{q=1}^{(\mathcal{I}_l)} R_{z \rightarrow (a,b)}^{(l)} M_{i,q}^{(l)}(a) M_{i+q,\lambda-q}^{(l)}(b) \\ &+ \sum_{a,b,c=1}^v \sum_{q,r=1}^{(\mathcal{I}_l)} R_{z \rightarrow (a,b,c)}^{(l)} M_{i,q}^{(l)}(a) M_{i+q,r}^{(l)}(b) M_{i+q+r,\lambda-q-r}^{(l)}(c) \end{aligned} \quad (15)$$

where we recall the level- $l$  rule probability tensors are equal to  $R_{z \rightarrow (a,b)}^{(l)} = 1/(2m_2)$  and  $R_{z \rightarrow (a,b,c)}^{(l)} = 1/(2m_3)$  if such rules are grammatical. We define the integer interval  $\mathcal{I}_l = [2^{L-l}, 3^{L-l}]$ : the span length  $\lambda$ , pertaining to level- $(l-1)$ , satisfies  $\lambda \in I_{l-1}$ , i.e. the integer interval  $[2^{L-l+1}, 3^{L-l+1}]$ . The summation over splits (illustrated in the sketch of Fig. 13)

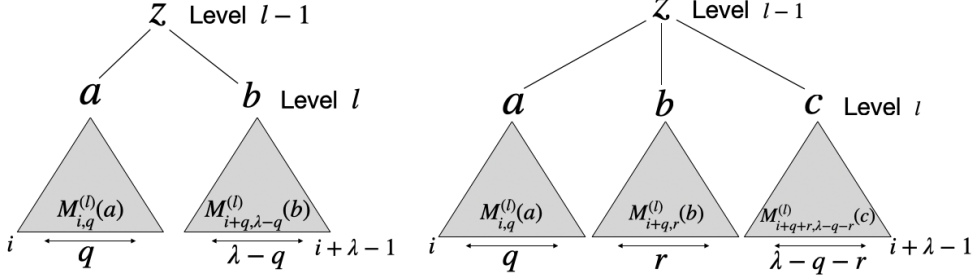


Figure 13. Sketch illustrating the notion of binary (left) and ternary (right) splits in the inside recursion, corresponding respectively to the first and second term in (15).

instead is restricted in the following manner, which we denote by the superscript  $(I_l)$ :

$$\sum_q^{(I_l)} f(q) := \sum_{\substack{q \in \mathbb{Z} \\ 2^{L-l} \leq q \leq 3^{L-l} \\ 2^{L-l} \leq \lambda - q \leq 3^{L-l}}} f(q) \quad (16)$$

$$\sum_{q,r}^{(I_l)} g(q,r) := \sum_{\substack{q,r \in \mathbb{Z} \\ 2^{L-l} \leq q, r \leq 3^{L-l} \\ 2^{L-l} \leq \lambda - q - r \leq 3^{L-l}}} g(q,r) \quad (17)$$

For example, when building the level- $(L-2)$  tensor, for  $\lambda = 6$  there is a single valid binary ( $q = 3$ ) and a single valid ternary ( $q = 2, r = 2$ ) split, corresponding respectively to the two ways of splitting a span of length 6 into segments of length 2 or 3, 3-3 or 2-2-2.

Filling in the whole inside tensor following a naive implementation of (15) quickly runs into computational limits, given that the loop over start positions, span lengths  $\lambda$  and splits leads to an  $\mathcal{O}(d^3)$  scaling for binary rules, and  $\mathcal{O}(d^4)$  for ternary. From a computational standpoint, the layerwise structure is indeed essential, as it enables efficient parallelization. The  $\mathcal{O}(d^4)$  time complexity scaling would make a naive implementation unfeasible already for  $L > 3$ ; by parallelizing, we are able to compute numerically up to  $L = 6$  (where  $d \sim \langle s \rangle^L \sim 244$  and  $! N_t \sim 10^{38}$ ) the expected class entropies  $\mathbb{E}_{x, \mathcal{G}}[H_L(\alpha | x)]$ .

To achieve this, we tensorize (15) (for fixed  $\lambda$ ) and parallelize the computation to fill in the next-level inside tensor. We can do this by defining a  $v \times v \times v$  size tensor for storing binary rule probabilities  $R_{z \rightarrow (a,b)}^{(l)}$ , and a  $v \times v \times v \times v$  for ternary  $R_{z \rightarrow (a,b,c)}^{(l)}$ . We further precompute the set of valid binary  $\{q\}$  and ternary  $\{(q, r)\}$  splits for each  $\lambda$ , the total number of which we can denote by  $N_{\text{bin}}(\lambda)$  and  $N_{\text{ter}}(\lambda)$  respectively. These are expected to grow as  $N_{\text{bin}}(\lambda) \sim \lambda$  and  $N_{\text{ter}}(\lambda) \sim \lambda^2$ . We confirm this in Fig. 14. Defining the reversed level index  $\tilde{l} = L - l$ , so that  $\tilde{l} = 0 \dots L$  from tokens to root, we show the median of the number of splits required to fill in the level- $\tilde{l}$  inside tensor, across the span lengths  $\lambda = 2^{\tilde{l}}, \dots, 3^{\tilde{l}}$ . The median is dominated by the maximum span length  $\sim 3^{\tilde{l}}$ .

The parallel computation involves (in the ternary case) building a tensor of shape  $d \times N_{\text{ter}}(\lambda) \times v \times v \times v \times v$ , which we sum over all but the first and third dimensions, leaving the  $d \times v$  elements needed to fill in the entries of the inside tensor at fixed span length for  $i = 1 \dots d$  and  $z = 1 \dots v$ . Due to memory constraints, for large  $\tilde{l}$  it can be prohibitive to parallelize simultaneously over the  $d \sim \langle s \rangle^L$  start positions and the  $N_{\text{ter}} \sim 3^{2\tilde{l}}$  splits. As we illustrate in Fig. 14 for  $L = 6$ , beyond a certain  $\tilde{l}$  ( $\tilde{l} = 4$  in this case)  $N_{\text{ter}}$  surpasses  $d$ , so that we in fact maintain the loop over start positions and only parallelize across splits. We note finally that for large  $L > 4$  we implement the inside algorithm (15) in log-probability space, to prevent underflow.

## B.2. Bottom-up theory for $f_c$

We here provide the improved estimate of the crossover point  $f_c = 3/8$ , stated in the main text. To this end, we consider a “coarse-grained” form of the inside algorithm (15), based on two simplifications. Firstly, we neglect fluctuations across the

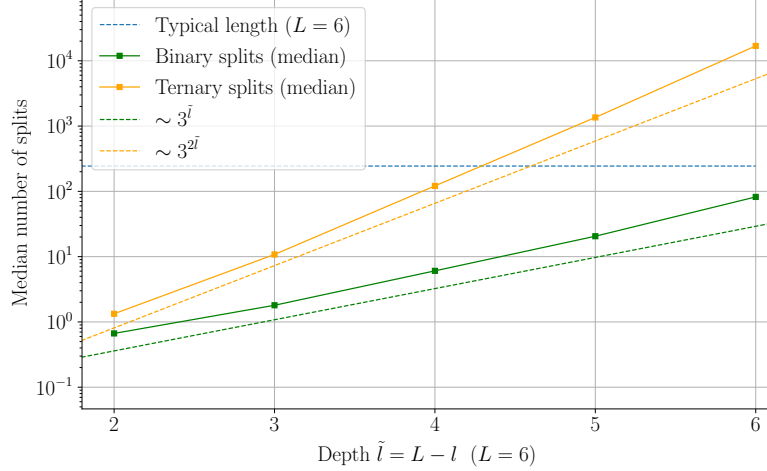


Figure 14. Median number of binary and ternary splits, required to build the inside tensor at depth  $\tilde{l}$ , across the span lengths  $\lambda \in [2^{\tilde{l}}, 3^{\tilde{l}}]$ . The medians are dominated by the tail, so that these grow as  $\sim 3^{\tilde{l}}$  for the binary and  $\sim 3^{2\tilde{l}}$  for the ternary case, as shown by dashed lines. For the example case of  $L = 6$ ,  $N_{\text{ter}}$  surpasses the sentence length  $d \sim \langle s \rangle^L$  beyond  $\tilde{l} = 4$ .

input dimension  $d$ , as well as boundary effects, which is a safe assumption for large enough  $L$  and hence  $d$ . Secondly, we get rid of the fine structure of the rules, which as shown in Sec. 4 is essential for learning, and instead simply keep track of how many candidate latents (both genuine and spurious) the inside algorithm builds on average across the vocabulary, as it proceeds up the hierarchy. More precisely, we consider the quantity

$$n_{\lambda}^{(l)} = \frac{1}{d} \sum_{i=1}^d \sum_{z=1}^v N_{i,\lambda}^{(l)}(z) \quad (18)$$

defined from the Boolean inside tensors  $N_{i,\lambda}^{(l)}$ . It is important to note that, although we continue to work in the  $v \rightarrow \infty$  limit, we *do not* scale (18) by  $v$ , and yet it is  $\mathcal{O}(1)$ . This is due to how the inside tensor is initialized. Indeed, the token-level inside tensor is initialized as  $N_{i,\lambda=1}^{(L)}(z) = \delta_{x_i,z}$ , so there is precisely one latent symbol across the vocabulary dimension, hence  $n_{\lambda=1}^{(L)} = 1$ .

We now consider the evolution of the average number of latents (18), both genuine and spurious, as the inside algorithm proceeds to build these layer by layer. This will be given by

$$n_{\lambda}^{(l-1)} = f_2 \sum_q^{(\mathcal{I}_l)} n_q^{(l)} n_{\lambda-q}^{(l)} + f_3 \sum_{q,r}^{(\mathcal{I}_l)} n_q^{(l)} n_r^{(l)} n_{\lambda-q-r}^{(l)} \quad (19)$$

which simply reflects the fact that, the way we have defined the model, once a binary split  $q$  is fixed, the pair of latents occupying that split correspond to a grammatical rule with probability  $f_2$ , and analogously in the ternary case. As in the main text, we consider for simplicity  $f_2=f_3=f$ .

In the case  $f=1$ , where all pairs/triples of candidate latents correspond to a grammatical rule, one expects that (19) will build as many latents as there are distinct tree topologies. In other words, at “depth”  $\tilde{l} = 0, \dots, L$ , i.e.  $\tilde{l} = L - l$ , and sentence length  $d = \lambda$ , we expect the following equality  $n_{\lambda=d}^{\tilde{l}=L} = N_t(d, L)$ . In Fig. 15 we confirm this equality numerically, by implementing Eq. 19 with  $f=1$  and comparing to  $N_t$  computed top-down from (11).

With  $f < 1$  instead, each time we try to place a new latent we weigh this by the probability of the pair/triple of level- $l$  latents to actually constitute a grammatical rule. Without the inclusion of additional terms, we expect (19) to recover again a bifurcation around  $f_c = 1/2$ , which we recall was obtained by balancing the number of tree topologies  $N_t$  with the fraction of grammatical data  $F$  (see App. A). For  $f > f_c$ ,  $n$  grows without bound for increasing depth, while for  $f < f_c$  it instead decays to zero. This is confirmed in Fig. 16.

To obtain an improved estimate of  $f_c$ , we must consider the main reason why (19) is problematic. This is the fact that, although we are simply considering *on average* how many latents are built, there is in fact a fraction of latents, the genuine

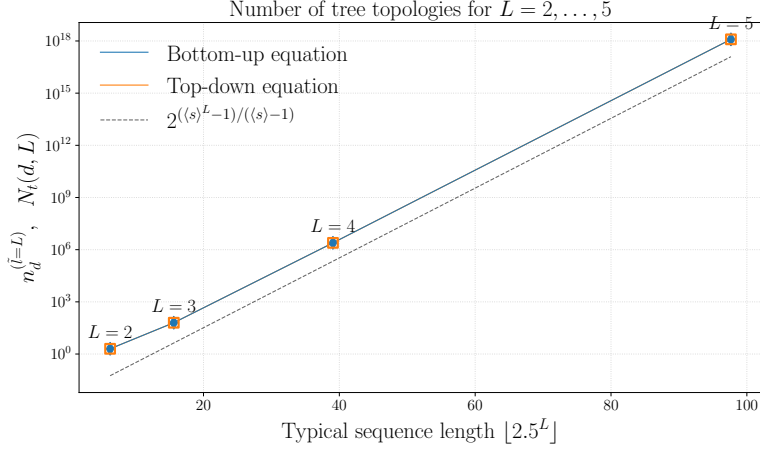


Figure 15. Comparison of  $n_{\lambda=d}^{(\tilde{l}=L)}$ , computed bottom-up from (19), and  $N_t(d, L)$ , obtained top-down from (11), evaluated at the typical sentence length  $d = \lfloor \langle s \rangle^L \rfloor$ , for  $L = 2, 3, 4, 5$ . These match exactly, and grow asymptotically as  $\sim 2^{(\langle s \rangle^L - 1) / (\langle s \rangle - 1)}$  (dashed lines).

ones (i.e. present on the true derivation tree), which follow a different dynamics. Their contribution to (19) in fact vanishes as we proceed up the hierarchy, but is still significant for  $l=L-1$ . The fact that they vanish can be seen from the following: their number is controlled by the average branching ratio, so that, if we decompose the contributions as  $n_\lambda^{(l)} = n_\lambda^{(l),\text{true}} + n_\lambda^{(l),\text{spurious}}$ ,

$$\sum_{\lambda=2^{L-l}}^{3^{L-l}} n_\lambda^{(l),\text{true}} = \frac{1}{\langle s \rangle^{L-l}} \quad (20)$$

At the level- $(L-1)$ , this is still a significant effect, while for  $l < L-1$  it can be quickly neglected. Therefore, to obtain an improved estimate of  $f_c$ , we start the layerwise mapping (19) instead one level above, using the *correct* initial condition which can be determined exactly at  $l=L-1$ . In other words, we account for the error committed by (19) in the first step of the hierarchy. The new initial condition is given by

$$n_\lambda^{(L-1)} = n_\lambda^{(L-1),\text{true}} + n_\lambda^{(L-1),\text{spurious}} = \frac{1}{2\langle s \rangle} + f \left( 1 - \frac{1}{2\langle s \rangle} \right) \quad (21)$$

for  $\lambda = 2, 3$ . The quantity (21) is, for any  $f < 1$ , larger than the value  $n_\lambda^{(L-1)} = f$  for  $\lambda = 2, 3$  predicted from the original evolution (19). Therefore, effectively the presence of genuine latents renormalizes the initial condition, making it larger. Starting the mapping (19) at level- $(L-1)$  using the corrected value (21), we obtain the improved prediction  $f_c = 3/8$ , simply from equating (21) to the known critical number  $n_{\lambda=2,3}^{(L-1)} = 1/2$ .

### B.3. Limitations

Although we expect the averaged dynamics of (19) to capture the crux of the crossover, and indeed the prediction  $f_c = 3/8$  is in qualitative agreement with the data (Fig. 3), we comment here on its limitations and what is missing in order to have a complete analytical theory of the class entropy curves  $\mathbb{E}[H_L(\alpha|x)]$ . A first important aspect is that, in deriving (19), we ignore boundary effects, which is a safe assumption when considering the average number across positions; however, the class entropy is controlled by a very specific entry of the inside tensor, namely the element  $N_{1,d}^{(0)}$  corresponding to a complete span. Therefore, there are additional boundary effects that need to be captured in order to obtain a quantitative class entropy prediction at any  $L$ . The second aspect connects to why we refer to this as a local-global ambiguity crossover, and not a sharp transition for large  $L$ . This is due to an additional effect not captured by (19), and is related to the special character of the root position alluded to above: namely, it is easy to show that the class entropy curves  $\mathbb{E}[H_L(\alpha|x)]$  are strictly growing with  $L$  at any  $f$ . It is clear intuitively, indeed, that the class entropy at depth  $L$  is bounded from below by the  $L=2$  value: even if the inside algorithm builds only the true candidates at the penultimate level  $l=2$ , one is still left with the expected class entropy for this  $L=2$  sentence.

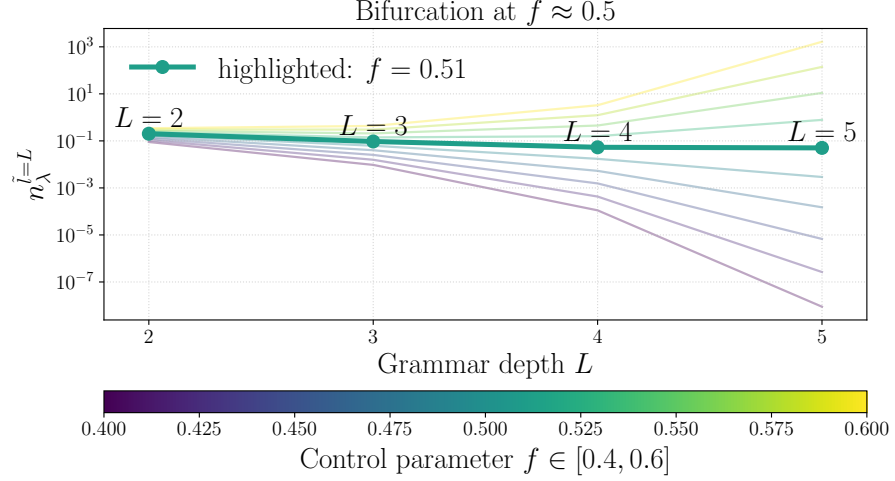


Figure 16. Numerical implementation of the iterative mapping (19) for  $n_{\lambda}^{(L)}$ , from the initial condition  $n_{\lambda=1}^{(L)} = 1$  and evaluated for each depth at the typical sentence length  $\lambda = \lfloor \langle s \rangle^L \rfloor$ . As expected, we recover the prediction  $f_c = 1/2$  from the simple top-down argument (main text).

## C. Details of the iterative learning algorithm

In this section, we describe in detail the steps of the learning algorithm and prove that, given an ordered sentence  $X = (X_1, \dots, X_d)$  generated from the varying-tree RHM in the asymptotic vocabulary size limit ( $v \rightarrow \infty$  with  $m_s = f_s v^{s-1}$  for  $s = 1, 2$ ) and in the globally unambiguous phase ( $f_2, f_3 < f_c$ ), it infers the root label  $X^{(0)} = \alpha(X)$ . The proof is based on the behavior of the various contributions to root-to-pair and root-to-triple covariances in the asymptotic limit. Many of these contributions are indeed negligible in the limit, which results in the possibility to isolate the contributions of the individual rules, thus inferring the generative model layer by layer. Throughout most of this section, we assume knowledge of the exact moments of the data distribution. We will discuss convergence of the empirical moments and sample complexity in subsection C.5.

### C.1. Preliminary: Asymptotic rules statistics, marginal distributions of terminal/nonterminal symbols and covariance with the root

This subsection collects useful results about the scales of various statistics of data generated by the varying-tree RHM in the asymptotic vocabulary size limit. Let  $\pi \in \Delta^{v-1}$  be the distribution of the root  $X^{(0)}$ . For a fixed leaf  $i$ , and levels  $\ell = 1, \dots, L$ , let  $s_\ell(i)$  be the arity of the  $\ell$ -th step along the root-to-leaf path. The parent-to-child transition matrices are (probability of the  $s$ -th child given the parent)

$$\left( P_s^{(\ell)} \right)_{a,b} := \mathbb{P} \left\{ X_s^{(\ell)} = a \mid X^{(\ell-1)} = b \right\}; \quad P_s^{(\ell)} = J + \Delta_s^{(\ell)}, \quad (22)$$

with

$$J = \mathbb{E}[P_s^{(\ell)}] = \frac{1}{v} \mathbf{1} \mathbf{1}^\top, \quad \mathbb{E}[\Delta_s^{(\ell)}] = 0, \quad \text{Var} \left[ \Delta_s^{(\ell)}(a, b) \right] = \frac{1}{v m_s} \left( 1 - \frac{1}{v} \right) \frac{v^s - m_s}{v^s - 1} \rightarrow \frac{1}{f v^s} + O\left(\frac{1}{v^{s+1}}\right), \quad (23)$$

The expectation symbol denoting average over draws of the RHM rules. The expectation of column  $\ell_2$ -norm and Frobenius norm of the  $\Delta_s$ ’ are (layer index  $\ell$  dropped to ease notation)

$$\mathbb{E} \left[ \left\| (\Delta_s)_{:,b} \right\|^2 \right] = v \text{Var} [\Delta_s(a, b)] \rightarrow \frac{1}{f v^{s-1}}, \quad \mathbb{E} \left[ \|\Delta_s\|_F^2 \right] = v^2 \text{Var} [\Delta_s(a, b)] \rightarrow \frac{v^{2-s}}{f}. \quad (24)$$

To understand fluctuations, note that, since the entries of  $\Delta_s$  follow the hypergeometric distribution, they are sub-Gaussian with variance proxy  $\text{Var} [\Delta_s(a, b)]$ . Hence, the scale of the 4-th moment is bounded by  $\text{Var} [\Delta_s(a, b)]^2 = O((m_s v)^{-2})$ . Cross-moments such as  $\text{Cov} [\Delta_s(a, b)^2, \Delta_s(a', b)^2]$  obey the same bound via Cauchy-Schwarz  $\text{Cov} [X, Y] \leq$

$\sqrt{\text{Var}[X]}\sqrt{\text{Var}[Y]}$ . Therefore,

$$\text{Var} \left[ \|(\Delta_s)_{:,b}\|^2 \right] = \text{Var} \left[ \sum_a \Delta_s(a,b)^2 \right] = \sum_a \text{Var} [\Delta_s(a,b)^2] + \sum_{a' \neq a} \text{Cov} [\Delta_s(a,b)^2, \Delta_s(a',b)^2] \leq O \left( \frac{1}{m_s^2} \right). \quad (25)$$

The Frobenius norm is the sum of the  $\ell_2$ -norms of the columns, hence we can bound its variance with the sum of the column norms' variances (the real variance is even smaller by the anti-correlations of the columns),

$$\text{Var} [\|\Delta_s\|_F^2] \leq \sum_v \text{Var} \left[ \|(\Delta_s)_{:,b}\|^2 \right] \leq O \left( \frac{v}{m_s^2} \right), \quad (26)$$

which implies concentration since the squared mean is  $O(v^2/m_s^2)$ . Sub-gaussianity of the entries with variance proxy  $O(1/(m_s v))$  also gives the operator norm via the circular law for the distribution of the eigenvalues of a  $v \times v$  random matrix with independent and identically distributed entries in the limit  $v \rightarrow \infty$ ,

$$\|\Delta_s\|_{\text{op}}^2 \rightarrow \frac{1}{m_s}, \quad \|\Delta_s\|_F^2 \rightarrow \frac{v}{m_s}. \quad (27)$$

It's not a surprise that the operator norm has the same scale as the  $\ell_2$ -norm of the columns, while it is smaller than the Frobenius norm by a factor of  $v$ : due to the symmetry for exchanging symbols, there is no preferred direction, thus the spectrum of  $\Delta_s$  is approximately flat.

**Average over child position.** We will also need the properties of

$$\tilde{\Delta}^{(\ell)} := p_2 \left( \frac{1}{2} \sum_{i=1}^2 \Delta_{2,i}^{(\ell)} \right) + p_3 \left( \frac{1}{3} \sum_{i=1}^3 \Delta_{3,i}^{(\ell)} \right). \quad (28)$$

The different  $\Delta$ 's appearing in this formula are all independent, because binary and ternary rules are sampled independently, and there are no correlations between the symbols in different positions on the right-hand side of a production rule. In addition, the statistics of the transition matrices are independent of the child index. Therefore,

$$\text{Var} [\tilde{\Delta}(a,b)] = \left( \frac{p_2}{2} \right)^2 2\text{Var} [\Delta_2(a,b)] + \left( \frac{p_3}{3} \right)^2 3\text{Var} [\Delta_3(a,b)] \rightarrow \frac{p_2^2}{2} \frac{1}{f v^2} + O \left( \frac{1}{v^3} \right). \quad (29)$$

All the conclusions on sub-gaussianity, Frobenius and operator norm apply to this case as well, with Eq. 29 variance proxy.

### C.1.1. ASYMPTOTIC MARGINALS OF TERMINALS AND NONTERMINALS

**Lemma C.1** (Asymptotic symbol marginals). *in the limit  $v \rightarrow \infty$  with  $f$  fixed and  $m_s = f v^{s-1}$  for  $s = 2, 3$ , the marginal probability of a single hidden (nonterminal) or visible (terminal) symbol converges to the uniform probability  $1/v$ .*

The leaf marginal is

$$p_i^{(L)} = \left( \prod_{\ell=1}^L P_{s_\ell(i)}^{(\ell)} \right) \pi = \left( \prod_{\ell=1}^L \left( J + \Delta_{s_\ell(i)}^{(\ell)} \right) \right) \pi. \quad (30)$$

Expanding the product and using  $J\Delta = 0$ ,  $J\pi = u$  (uniform distribution  $\mathbf{1}/v$ ),  $Ju = u$ ,

$$p_i^{(L)} = u + \sum_{r=2}^L \left( \Delta_{s_L(i)}^{(L)} \cdots \Delta_{s_r(i)}^{(r)} \right) u + \left( \Delta_{s_L(i)}^{(L)} \cdots \Delta_{s_1(i)}^{(1)} \right) \pi. \quad (31)$$

**Ensemble mean (uniform).** By independence and  $\mathbb{E}[P_{s_\ell}^{(\ell)}] = J$ ,

$$\mathbb{E}[p_i^{(L)}] = \left( \prod_{\ell=1}^L \mathbb{E}[P_{s_\ell(i)}^{(\ell)}] \right) \pi = J^L \pi = \frac{1}{v} \mathbf{1}. \quad (32)$$

**Concentration.** Write  $p_i^{(\ell)}$  for the leaf distribution after  $\ell$  steps on the path, with  $p^{(0)} = \pi$  and  $\delta_i^{(\ell)} = p_i^{(\ell)} - u$ . Using  $Jp = u$  for any distribution  $p \in \Delta^{v-1}$  (second equality),

$$\delta_i^{(\ell)} = P_{s_\ell(i)}^{(\ell)} p_i^{(\ell-1)} - u = \left( P_{s_\ell(i)}^{(\ell)} - J \right) p_i^{(\ell-1)} = \Delta_{s_\ell(i)}^{(\ell)} u + \Delta_{s_\ell(i)}^{(\ell)} \delta_i^{(\ell-1)}. \quad (33)$$

Conditioning on  $\delta^{(\ell-1)}$  and using independence of the levels, (path index  $i$  omitted for simplicity)

$$\mathbb{E} \left[ \|\delta^{(\ell)}\|_2^2 \mid \delta^{(\ell-1)} \right] = p^{(\ell-1)\top} \mathbb{E} \left[ \Delta_s^{(\ell)\top} \Delta_s^{(\ell)} \right] p^{(\ell-1)} = \left( u + \delta^{(\ell-1)} \right)^\top G_s \left( u + \delta^{(\ell-1)} \right). \quad (34)$$

The statistics of the centred transition probabilities,  $\Delta_{a,b} = P_{a,b} - \mathbb{E}[P_{a,b}]$ , are invariant for permutations of the indices. As a result,

$$G_s := \mathbb{E} [\Delta_s^\top \Delta_s] := \alpha_s I_v + \beta_s (\mathbf{1}\mathbf{1}^\top - I_v), \quad (35)$$

where  $\alpha_s$  denotes the diagonal entries and  $\beta_s$  the off-diagonal ones,

$$\alpha_s := \sum_{a=1}^v \text{Var}(P_s(a,c)) = \frac{1}{m_s} \left( 1 - \frac{1}{v} \right) \frac{v^s - m_s}{v^s - 1} = \frac{1}{fv^{s-1}} + O\left(\frac{1}{v^s}\right), \quad (36)$$

$$\beta_s := \sum_a \text{Cov}(P_s(a,c), P_s(a,c')) = -\frac{1}{v} \frac{v-1}{v^s-1} = -\frac{1}{v^s} + O\left(\frac{1}{v^{s+1}}\right). \quad (37)$$

$G_s$  is a rank-1 perturbation of the identity, hence we can derive its spectrum by decomposing it along the rank-1 component  $J = \mathbf{1}\mathbf{1}^\top/v$  and the orthogonal subspace spanned by  $I_v - J$ ,

$$\begin{aligned} G_s &= (\alpha_s - \beta_s) I_v + v\beta_s J = (\alpha_s - \beta_s) (I_v - J) + (\alpha_s + (v-1)\beta_s) J \\ &= \lambda_s^{(\parallel)} J + \lambda_s^{(\perp)} (I_v - J), \end{aligned} \quad (38)$$

whence

$$\lambda_s^{(\perp)} = \alpha_s - \beta_s = \frac{1}{fv^{s-1}} + O\left(\frac{1}{v^s}\right), \quad \lambda_s^{(\parallel)} = \alpha_s + (v-1)\beta_s = \frac{1-f}{fv^{s-1}} + O\left(\frac{1}{v^s}\right). \quad (39)$$

Hence, after averaging over  $\delta^{(\ell-1)}$  (and reinstating the dependence on the arity of the level  $s$ ),

$$\mathbb{E} \left[ \|\delta^{(\ell)}\|_2^2 \right] = \lambda_{s,\perp} \mathbb{E} \left[ \|\delta^{(\ell-1)}\|_2^2 \right] + \frac{\lambda_{s,\parallel}}{v}, \quad (40)$$

which yields

$$\mathbb{E} \|\delta^{(L)}\|_2^2 = \left( \prod_{\ell=1}^L \lambda_{s_\ell}^{(\perp)} \right) \|\pi - u\|_2^2 + \frac{1}{v} \sum_{r=1}^L \lambda_{s_r}^{(\parallel)} \prod_{\ell=r+1}^L \lambda_{s_\ell}^{(\perp)}. \quad (41)$$

As  $v \rightarrow \infty$  for fixed  $f$  ( $m_s = fv^{s-1}$ ),

$$\lambda_s^{(\perp)} = \frac{1}{fv^{s-1}} + O(v^{-s}), \quad \lambda_s^{(\parallel)} = \frac{1-f}{f} v^{-(s-1)} + O(v^{-s}) \quad (42)$$

$$\Rightarrow S = \sum_{\ell=1}^L (s_\ell - 1) : \quad \prod_{\ell=1}^L \lambda_{s_\ell}^{(\perp)} = \frac{1}{f^L v^S} \left( 1 + O(v^{-1}) \right), \quad (43)$$

$$\Rightarrow \mathbb{E} \|\delta^{(L)}\|_2^2 = \frac{\|\pi - u\|_2^2}{f^L v^S} + \frac{1-f}{f} v^{-s_L} + O(v^{-\min\{S+1, s_L+1\}}). \quad (44)$$

When the root prior is uniform, fluctuations are controlled by the arity of the last level  $s_L$ :  $v^{-2}$  or  $v^{-3}$ . By invariance of the rules' statistics for permutations of the indices,

$$\mathbb{E} \left[ \left( \left( p_i^{(L)} \right)_a - \frac{1}{v} \right)^2 \right] = \frac{\mathbb{E} \left[ \|\delta_i^{(L)}\|_2^2 \right]}{v} \rightarrow \frac{1-f}{f} \frac{1}{v^{s_L+1}}. \quad (45)$$

The variance decays faster than the squared mean  $v^{-2}$  with  $v$ , independently of the arity. Therefore, the leaf marginals concentrate around the uniform distribution. Considering a random leaf instead of a well-defined path with specific arities  $s_\ell$  at all levels does not change the result, since the marginals converge to the uniform distribution regardless.

## C.1.2. ROOT-TO-TERMINAL AND ROOT-TO-NONTERMINAL COVARIANCES

In this section, we consider the covariance between the root  $X^{(0)}$  and a single nonterminal or terminal symbol. The size of the elements of this covariance matrix is crucial for determining the size of the various contributions to root-to-pair and root-to-triple covariances. For a fixed terminal  $i$ , and levels  $\ell = 1, \dots, L$ , let  $s_\ell(i)$  be the arity of the  $\ell$ -th step along the path. Define the root-to-terminal covariance with position  $i$  as

$$\begin{aligned} C^{(L)}(i; a, b) &:= \mathbb{P}\left\{X_i = a, X^{(0)} = b\right\} - \mathbb{P}\left\{X_i = a\right\} \mathbb{P}\left\{X^{(0)} = b\right\} \\ &= \sum_c \mathbb{P}\left\{X_i = a \mid X^{(0)} = c\right\} \left( \delta_{c,b} \mathbb{P}\left\{X^{(0)} = b\right\} - \mathbb{P}\left\{X^{(0)} = c\right\} \mathbb{P}\left\{X^{(0)} = b\right\} \right) \\ &\Rightarrow C^{(L)}(i) = P_{s_L(i)}^{(L)} \cdots P_{s_1(i)}^{(1)} \Sigma_\pi, \quad \text{with} \quad \Sigma_\pi = \text{diag}(\pi) - \pi\pi^\top. \end{aligned} \quad (46)$$

After decomposing each  $P$  as  $J + \Delta$  and noting that  $\mathbf{1}^\top \Sigma_\pi = 0$  thus  $J\Sigma_\pi = 0$ ,

$$C^{(L)}(i) = \left( \Delta_{s_L(i)}^{(L)} \cdots \Delta_{s_1(i)}^{(1)} \right) \Sigma_\pi. \quad (47)$$

We now define the root-to-terminal covariance with randomized position  $i$ . By construction, choosing a position uniformly among all terminals is equivalent to, at each depth  $\ell$ : (i) drawing the arity  $s_\ell \in \{2, 3\}$  (according to the model), and (ii) drawing the child index  $i$  uniformly from  $\{1, \dots, s_\ell\}$ . We first average over the child index for a *fixed* arity  $s_\ell$ , then over arities,

$$\tilde{\Delta}^{(\ell)} := \mathbb{E}_{s_\ell}[\bar{\Delta}^{(\ell)}] = p_2 \left( \frac{1}{2} \sum_{i=1}^2 \Delta_{2,i}^{(\ell)} \right) + p_3 \left( \frac{1}{3} \sum_{i=1}^3 \Delta_{3,i}^{(\ell)} \right). \quad (48)$$

Consequently,

$$C_1^{(L)} = \left( \prod_{\ell=1}^L \tilde{\Delta}^{(\ell)} \right) \Sigma_\pi. \quad (49)$$

**Lemma C.2** (Asymptotic root-to-terminal covariance). *in the limit  $v \rightarrow \infty$  with  $f$  fixed and  $m_s = fv^{s-1}$  for  $s=2, 3$ , operator and Frobenius norm of the root-to-terminal covariance matrix concentrate,*

$$\|C_1^{(L)}\|_{\text{op}}^2 \rightarrow \frac{1}{v^2} \frac{(p_2^2/2)^L}{(fv)^L}, \quad \|C_1^{(L)}\|_F^2 \rightarrow \frac{1}{v} \frac{(p_2^2/2)^L}{(fv)^L} \quad \left( C_1^{(L)}(a, b)^2 = O\left(\frac{1}{v^3} \frac{(p_2^2/2)^L}{(fv)^L}\right) \right). \quad (50)$$

For  $L=1$ , these scales agrees with those of  $\tilde{\Delta}_s$  from Eq. 28, approximately equal to  $v \times C_1^{(1)}$  by the asymptotic uniformity of the marginal distributions. As is the case for  $\tilde{\Delta}_s$ , the operator norm is smaller than the Frobenius norm by a factor  $v$ , and it can be shown to coincide asymptotically with the  $\ell_2$ -norm of the columns, signaling again a flat spectrum (reasonable due to the symmetry of the rules' distribution for exchanging symbols).

We first get a scale for the Frobenius norm by averaging over grammars,

$$\mathbb{E} \left[ \|C_1^{(L)}\|_F^2 \right] = \text{Tr} \left( \Sigma_\pi \mathbb{E} \left[ \left( \tilde{\Delta}^{(L)} \cdots \tilde{\Delta}^{(0)} \right)^\top \left( \tilde{\Delta}^{(L)} \cdots \tilde{\Delta}^{(0)} \right) \right] \Sigma_\pi \right) = \text{Tr} \left( \Sigma_\pi \left( \prod_{\ell=1}^L \tilde{G} \right) \Sigma_\pi \right), \quad (51)$$

where  $\tilde{G} = \mathbb{E} \left[ \tilde{\Delta}^\top \tilde{\Delta} \right]$ . All the  $\Delta$ 's appearing in  $\tilde{\Delta}$  are independent of each other. Thus,

$$\begin{aligned} \tilde{G} &= \left( \frac{p_2}{2} \right)^2 \left( \sum_{i=1}^2 \mathbb{E} [\Delta_{2,i}^\top \Delta_{2,i}] \right) + \left( \frac{p_3}{3} \right)^2 \left( \sum_{i=1}^3 \mathbb{E} [\Delta_{3,i}^\top \Delta_{3,i}] \right) = \frac{p_2^2}{2} G_2 + \frac{p_3^2}{3} G_3 \\ &= \tilde{\lambda}_\parallel J + \tilde{\lambda}_\perp (I_v - J), \end{aligned} \quad (52)$$

whence

$$\tilde{\lambda}_\perp = \frac{p_2^2}{2} \lambda_2^{(\perp)} + \frac{p_3^2}{3} \lambda_3^{(\perp)} = \frac{p_2^2}{2} \frac{1}{fv} + O\left(\frac{1}{v^3}\right), \quad \tilde{\lambda}_\parallel = \frac{p_2^2}{2} \lambda_2^{(\parallel)} + \frac{p_3^2}{3} \lambda_3^{(\parallel)} = \frac{p_2^2}{2} \frac{1-f}{fv} + O\left(\frac{1}{v^3}\right). \quad (53)$$

Since  $\Sigma_\pi \mathbf{1} = 0$ , only the  $\perp$  subspace contributes, giving

$$\mathbb{E} \left[ \|C_1^{(L)}\|_F^2 \right] = \left( \tilde{\lambda}_\perp \right)^L \|\Sigma_\pi\|_F^2 \rightarrow \frac{(p_2^2/2)^L}{v(fv)^L}. \quad (54)$$

Concentration about the mean Frobenius norm follows from the sub-gaussianity of the  $\tilde{\Delta}$ 's and the resulting concentration of the  $\tilde{\Delta}$ 's Frobenius norms. We can also get a scale for the operator norm by submultiplicativity,

$$\|C_1^{(L)}\|_{\text{op}} \leq \|\Sigma_\pi\|_{\text{op}} \prod_{\ell=0}^{L-1} \|\tilde{\Delta}^{(\ell)}\|_{\text{op}}. \quad (55)$$

In fact, there is a matching lower bound obtained by studying the  $\ell_2$ -norm  $\|C_1^{(L)}x\|_2$  for some random unitary  $x \in \mathbb{R}^v$ , which can be computed iteratively by showing that each additional level induces a gain of order  $\|\tilde{\Delta}\|_F/\sqrt{v} \simeq \|\tilde{\Delta}\|_{\text{op}}$ . Therefore, using  $\|\Sigma_\pi\|_{\text{op}} \rightarrow 1/v$  and  $\|\tilde{\Delta}\|_{\text{op}} \rightarrow \tilde{\lambda}_\perp$ ,

$$\|C_1^{(L)}\|_{\text{op}}^2 = \left( \tilde{\lambda}_\perp \right)^L \|\Sigma_\pi\|_{\text{op}}^2 \rightarrow \frac{(p_2^2/2)^L}{v^2(fv)^L} = \frac{\mathbb{E} \left[ \|C_1^{(L)}\|_F^2 \right]}{v}. \quad (56)$$

## C.2. Infer binary rules from the root-to-pair covariance (Step 2)

In this section, we prove that the covariance between root and pairs of adjacent tokens defined in [Eq. 2](#) is dominated by the contribution of binary siblings in the asymptotic vocabulary size limit. This results guarantees the validity of the clustering procedure described in [subsection 4.1](#) for the inference of level- $L$  binary rules.

Consider the leaf sequence  $\mathbf{X} = (X_1, \dots, X_d)$  and a uniformly random adjacent index  $I \in \{1, \dots, d-1\}$ . For a fixed pair  $(a, b) \in \mathcal{V}^2$ , define

$$X_{a,b}^{(L, \text{pair})} := \mathbb{E}[\mathbf{1}\{(X_I, X_{I+1}) = (a, b)\} \mid \mathbf{X}] = \frac{1}{d-1} \sum_{i=1}^{d-1} \mathbf{1}\{(X_i, X_{i+1}) = (a, b)\}. \quad (57)$$

We study the covariance  $C_2^{(L)}$  of  $X_{a,b}^{(L, \text{pair})}$  with the root one-hot vector,  $X^{(0)}$ . Given  $(a, b)$ , this covariance is a vector in  $\mathbb{R}^v$  with one component per possible root symbol  $\alpha$ . Assuming root prior probability  $\pi$ ,

$$C_2^{(L)}(a, b) := \text{Cov}(X_{a,b}^{(L, \text{pair})}, X^{(0)}) = \mathbb{E}[X_{a,b}^{(L, \text{pair})} X^{(0)\top}] - \mathbb{E}[X_{a,b}] \pi^\top \quad (\in \mathbb{R}^v). \quad (58)$$

To average over trees and positions, we partition by the type of the lowest common ancestor (LCA) of  $(X_U, X_{U+1})$  as illustrated in [Fig. 5](#): (bin) level- $(L-1)$  with binary rule (i.e.  $(X_U, X_{U+1})$  are binary siblings), (ter) level- $(L-1)$  with ternary rule (i.e.  $(X_U, X_{U+1})$  are ternary siblings) (cross,  $\ell$ ) LCA of level  $0 \leq \ell \leq L-2$  (i.e.  $(X_U, X_{U+1})$  sit across the boundary between input tuples). By the law of total covariance,

$$\begin{aligned} \text{Cov}(X_{a,b}^{(L, \text{pair})}, X^{(0)}) &= \mathbb{E} \left[ \text{Cov}(X_{a,b}^{(L, \text{pair})}, X^{(0)}) \mid \text{type(LCA)} \right] + \\ &\quad \text{Cov} \left( \mathbb{E} \left[ X_{a,b}^{(L, \text{pair})} \mid \text{type(LCA)} \right], \mathbb{E} \left[ X^{(0)} \mid \text{type(LCA)} \right] \right). \end{aligned} \quad (59)$$

Since the root is independent of  $\text{type(LCA)}$ ,  $\mathbb{E} \left[ X^{(0)} \mid \text{type(LCA)} \right]$  equals the root prior deterministically, and the second term on the right-hand side above vanishes. For the binary and both ternary terms, the type of the last production rule is

fixed. Hence, we can factorize these terms into a factor depending purely on the level- $L$  rules tensor, and a root-to-level- $(L-1)$ -nonterminal covariance,

$$\begin{aligned}\text{Cov}\left(X_{a,b}^{(L,\text{pair})}, X_{\alpha}^{(0)} \middle| \text{type(LCA)} = \text{bin}\right) &= \sum_{z=1}^v R_{z \rightarrow (a,b)}^{(L)} C_1^{(L-1)}(z, \alpha), \\ \text{Cov}\left(X_{a,b}^{(L,\text{pair})}, X_{\alpha}^{(0)} \middle| \text{type(LCA)} = \text{ter}\right) &= \sum_{z=1}^v \sum_{c=1}^v \left(R_{z \rightarrow (a,b,c)}^{(L)} + R_{z \rightarrow (c,a,b)}^{(L)}\right) C_1^{(L-1)}(z, \alpha).\end{aligned}\quad (60)$$

Finally, denoting with  $p_{\text{bin}}$ ,  $p_{\text{ter}}$  and  $p_{\text{cross}}$  the probabilities of the different LCA types,

$$\begin{aligned}\text{Cov}\left(X_{a,b}^{(L,\text{pair})}, X_{\alpha}^{(0)}\right) &= p_{\text{bin}} \sum_{z=1}^v R_{z \rightarrow (a,b)}^{(L)} C_1^{(L-1)}(z, \alpha) + p_{\text{ter}} \sum_{z=1}^v \sum_{c=1}^v \left(R_{z \rightarrow (a,b,c)}^{(L)} + R_{z \rightarrow (c,a,b)}^{(L)}\right) C_1^{(L-1)}(z, \alpha) \\ &\quad + p_{\text{cross}} C_{(a,b),\alpha}^{\text{cross}},\end{aligned}\quad (61)$$

**Binary contribution and clustering.** The binary contribution consists of the matrix product between the  $v^2$ -by- $v$  binary rules tensor  $R_{z \rightarrow (a,b)}^{(L)}$  and the root-to-nonterminal covariance matrix  $C_1^{(L-1)}(z, \alpha)$ , whose entries have typical size given by [Theorem C.2](#) in the asymptotic limit. For every pair  $(a, b)$  of binary siblings,  $R_{z \rightarrow (a,b)}^{(L)}$  selects the unique  $z(a, b)$  that generates the pair via a binary rule. Therefore, the size of these entries is given by

$$C_2^{(L,\text{bin})}((a, b), \alpha) = \frac{1}{m_2} C_1^{(L-1)}(z(a, b), \alpha) \rightarrow O\left(\frac{1}{fv} \sqrt{\frac{1}{v^3} \frac{(p_2^2/2)^{L-1}}{(fv)^{L-1}}}\right), \quad (62)$$

whereas the binary contribution vanishes on pairs  $(a, b)$  that are not binary siblings. While the other terms might be nonzero on such pairs, their size is negligible with respect to [Eq. 62](#) for large  $v$ , implying the identifiability of the valid binary siblings.

**The ternary contribution is negligible.** The ternary contribution can be written as the product of a level- $L$  kernel  $K_{(a,b),z}^{(\text{ter})}$  and the root-to-nonterminal covariance matrix  $C_1^{(L-1)}(z, \alpha)$ . The kernel reads

$$\begin{aligned}K_{(a,b),z}^{(\text{ter})} &= \sum_c \frac{1}{2} \left( \mathbb{P}\left\{(X_U, X_{U+1}, X_{U+2}) = (a, b, c) \middle| X_U^{(L-1)} = z\right\} + \mathbb{P}\left\{(X_{U-1}, X_U, X_{U+1}) = (c, a, b) \middle| X_U^{(L-1)} = z\right\} \right) \\ &= \frac{1}{2} \left( \left(P_{3,(12)}^{(L)}\right)_{(a,b),z} + \left(P_{3,(23)}^{(L)}\right)_{(a,b),z} \right),\end{aligned}\quad (63)$$

where  $P_{3,(ij)}^{(L)}$  denotes the ternary rules parent-to-child  $v^2 \times v$  transition matrix with children positions  $i$  and  $j$ . By generalising [Eq. 22](#) and [Eq. 23](#),

$$P_{3,(ij)}^{(L)} = \frac{1}{v^2} \mathbf{1}_{v^2} \mathbf{1}_v^\top + \Delta_{3,(ij)}^{(L)}, \quad \text{with} \quad \mathbb{E}[\Delta_{3,(ij)}^{(L)}] = 0, \quad \text{Var}[\Delta_{3,(ij)}^{(L)}] = \frac{1}{v^2 m_3} \left(1 - \frac{1}{v^2}\right) \frac{v^3 - m_3}{v^3 - 1} \rightarrow \frac{1}{fv^4}. \quad (64)$$

The decay in the covariance's square norm due to the transition is given by  $v \times$  the variance above (the scale of  $\lambda_\perp$ , or  $\|\Delta\|_F^2/v$ , or  $\|\Delta\|_{\text{op}}^2$ ), so that the size of the ternary contribution is that of  $C_1^{(L-1)}$  times  $(fv^3)^{-1/2}$ . For any finite  $f$ , this is sub-leading with respect to the  $(fv)^{-1}$  scaling of the binary term.

**The cross contribution is negligible.** All the other contributions consist of a root-to-nonterminal covariance over  $\ell \leq L-2$  layers,  $C_1^{(\ell)}$ , then a binary transition and two branches from the children of this transition to the terminal symbols. This term is necessarily smaller than the others because, even with  $\ell = L-2$ , it contains an extra transition at the last level (the second branch), adding another factor of  $(fv)^{-1}$  to the covariance's size.

### C.3. Infer ternary rules from the (whitened) root-to-triple covariance (Step 3)

In this section, we prove that the covariance between root and triples of adjacent tokens defined in [Eq. 3](#) is given, in the asymptotic vocabulary size limit, by the contribution of ternary siblings plus spurious contributions from binary siblings

that are proportional to the root-to-pair covariance  $C_2^{(L)}$ . This result guarantees the validity of the procedure described in subsection 4.2 for the inference of level- $L$  ternary rules.

As in subsection C.2, given a sequence  $\mathbf{X}$  and a random index  $I \in \{1, \dots, d-2\}$ , fix a triple  $(a, b, c) \in \mathcal{V}^3$  and define

$$X_{a,b,c}^{(L,\text{triple})} := \mathbb{E}[\mathbf{1}\{(X_I, X_{I+1}, X_{I+2}) = (a, b, c) | \mathbf{X}\}] = \frac{1}{d-2} \sum_{i=1}^{d-2} \mathbf{1}\{(X_i, X_{i+1}, X_{i+2}) = (a, b, c)\}, \quad (65)$$

The root-to-triple covariance is the  $v \times v \times v \times v$  covariance tensor between  $X^{(L,\text{triple})}$  and the root one-hot vector  $X^{(0)}$ , or a vector in  $\mathbb{R}^v$  per triple  $(a, b, c)$ . Following subsection C.2, we use the law of total covariance to decompose the covariance into contributions corresponding to different local topologies (see Fig. 5 for an illustration). The three terminal symbols selected can share the same LCA at level  $L-1$  (i.e. they are ternary siblings, probability  $p_{\text{ter}}$ ) or only two of the three (either  $(a, b)$  or  $(b, c)$  with the same probability) come from the same level- $(L-1)$  nonterminal. In the latter case, the two terminals sharing the LCA are either binary (probability  $p_{\text{bin}}$ ) or ternary siblings (probability  $p_{\text{ter}}$ ). Therefore,

$$\begin{aligned} C_{(a,b,c),r}^{\text{triple}} &= p_{\text{ter}} \sum_z R_{(a,b,c),z}^{(L,\text{ter})} C_{z,r}^{(L-1)} \\ &+ \sum_z \left( p_{\text{bin}} R_{z \rightarrow (a,b)}^{(L,\text{bin})} + p_{\text{ter}} \sum_d R_{z \rightarrow (d,a,b)}^{(L,\text{ter})} \right) \sum_{z'} P_{z' \rightarrow c}^{(L)} C_{(z,z'),\alpha}^{(L-1)} \\ &+ \sum_z P_{z \rightarrow a}^{(L)} \sum_{z'} \left( p_{\text{bin}} R_{z' \rightarrow (b,c)}^{(L,\text{bin})} + p_{\text{ter}} \sum_d R_{z' \rightarrow (b,c,d)}^{(L,\text{ter})} \right) C_{(z,z'),\alpha}^{(L-1)}, \end{aligned} \quad (66)$$

where  $P_{z' \rightarrow c}^{(L)}$  and  $P_{z \rightarrow a}^{(L)}$  are nothing but parent-to-child transition matrices from Eq. 22.<sup>1</sup>

**Ternary contribution.** The pure ternary contribution consists of the matrix product between the  $v^3$ -by- $v$  ternary rules tensor  $R_{z \rightarrow (a,b,c)}^{(L)}$  and the root-to-nonterminal covariance matrix  $C_1^{(L-1)}(z, \alpha)$ , whose entries have typical size given by Theorem C.2 in the asymptotic limit. As in the binary rules tensor, for every pair  $(a, b, c)$  of ternary siblings,  $R_{z \rightarrow (a,b,c)}^{(L)}$  selects the unique  $z(a, b, c)$  that generates the triple via a ternary rule. Therefore, the size of these entries is given by

$$C_3^{(L,\text{ter})}((a, b, c), \alpha) = \frac{1}{m_3} C_1^{(L-1)}(z(a, b, c), \alpha) \rightarrow O\left(\frac{1}{fv^2} \sqrt{\frac{1}{v^3} \frac{(p_2^2/2)^{L-1}}{(fv)^{L-1}}}\right), \quad (67)$$

whereas it vanishes on triples  $(a, b, c)$  that are not ternary siblings. Due to the dependence on the nonterminal  $z(a, b, c)$ , the direction of the  $v$ -dimensional vector  $C_3^{(L,\text{ter})}((a, b, c), :)$  can be used to cluster triples by the generating nonterminals.

**Binary contributions.** We will only consider the binary contribution due to  $(a, b)$  coming from the same level- $(L-1)$  nonterminal, as the other is identical in size and statistics. By writing  $P^{(L)}$  ad  $J + \Delta$ , we get

$$\begin{aligned} &\sum_z \left( p_{\text{bin}} R_{z \rightarrow (a,b)}^{(L,\text{bin})} + p_{\text{ter}} \sum_d R_{z \rightarrow (d,a,b)}^{(L,\text{ter})} \right) \sum_{z'} P_{z' \rightarrow c}^{(L)} C_{(z,z'),\alpha}^{(L-1)} \\ &= \sum_z \left( p_{\text{bin}} R_{z \rightarrow (a,b)}^{(L,\text{bin})} + p_{\text{ter}} \sum_d R_{z \rightarrow (d,a,b)}^{(L,\text{ter})} \right) \left( \frac{1}{v} \sum_{z'} C_{(z,z'),\alpha}^{(L-1)} + \sum_{z'} \Delta_{c,z'}^{(L)} C_{(z,z'),\alpha}^{(L-1)} \right) \\ &\approx \frac{1}{v} C_2^{(L)}((a, b), \alpha) + \sum_z \left( p_{\text{bin}} R_{z \rightarrow (a,b)}^{(L,\text{bin})} + p_{\text{ter}} \sum_d R_{z \rightarrow (d,a,b)}^{(L,\text{ter})} \right) \left( \sum_{z'} \Delta_{c,z'}^{(L)} C_{(z,z'),\alpha}^{(L-1)} \right), \end{aligned} \quad (68)$$

where, in the last line, we neglected the cross contribution to the root-to-pair covariance, which is shown to vanish in the asymptotic vocabulary size limit in subsection C.2. Given the size of  $C_2^{(L)}$ 's entries from Eq. 62 ( $O(v^{-L/2-2})$ ), we have that, if  $(a, b)$  are valid binary siblings,  $v^{-1} C_2^{(L)}$  competes with the ternary contribution ( $O(v^{-L/2-3})$ ) in the asymptotic

<sup>1</sup>Note that the topology enforces the condition that the symbol  $c$  (resp.  $a$ ) is located on the left (resp. right) of its span, fixing the child position in the tensor. However, this property does not affect the conclusions of this section, and we will ignore it.

limit and cannot be neglected. The  $v^{-1}C_2^{(L)}((a, b), :)$  contribution to the root-to-triple vector  $C_3^{(L)}((a, b, c), :)$  hinders clustering because, for all triples  $(a, b, c)$  where  $(a, b)$  is generated by the same nonterminal  $z(a, b)$ , it aligns along a direction depending on  $z(a, b)$ . However, this term can be simply subtracted using the root-to-pair correlations computed in the previous step. The  $\Delta$ -dependent term is also similar in size, as  $C_2^{(L-1)}/m_2 = O(v^{-L/2-2})$  gets reduced by a further factor of  $1/m_2 = O(v^{-1})$  upon multiplication by the  $\Delta$  matrix. Although the  $\Delta$ -dependent binary contribution can be comparable in norm to the ternary signal, it varies with both the binary parent  $z(a, b)$  and the terminal symbol  $c$ , therefore it produces directions that decorrelate across triples sharing the same ternary nonterminal. As a result, this term acts as zero-mean directional noise and does not interfere with the inference of ternary rules.

#### C.4. Iteration and spurious nonterminals (Steps 4 and 5)

##### C.4.1. STEP 4: ESTIMATE ROOT-TO-PAIR- AND TRIPLE-OF-NONTERMINALS COVARIANCES

Once the level- $L$  rules are identified, we can fill in the Boolean inside tensor as  $N_{i,\lambda}^{(L-1)}(z) = 1$  whenever a rule with parent nonterminal  $z$  is detected at the span  $(i, \lambda)$ . Note that this tensor is defined and constructed for each sequence  $\mathbf{X}$ :

$$N_{i,\lambda}^{(L-1)}(z \mid \mathbf{X}) = \mathbf{1} \left\{ X_{i,\lambda}^{(L-1)} = z \right\} = \mathbf{1} \left\{ (X_i, \dots, X_{i+\lambda-1}) = (a_1, \dots, a_{\lambda-1}) \text{ with } R_{z \rightarrow (a_1, \dots, a_{\lambda-1})}^{(L)} \neq 0 \right\}. \quad (69)$$

In equations, this is done simply by considering the Boolean form of the inside algorithm (15), i.e. CYK. Let us define  $\tilde{R}_{z \rightarrow (a,b,c)}^{(\ell)}$  and  $\tilde{R}_{z \rightarrow (a,b,c)}^{(\ell)}$  as Boolean indicators for binary and ternary level- $\ell$  rules. After initializing the level- $L$  (leaf) indicators,

$$N_{i,1}^{(L)}(a \mid \mathbf{X}) = \mathbf{1} \{X_i = a\}, \quad N_{i,\lambda}^{(L)}(a \mid \mathbf{X}) = 0 \text{ for all } \lambda \geq 2, \quad (70)$$

we get (see App. B for notation)

$$\begin{aligned} N_{i,\lambda}^{(\ell-1)}(z) &= \sum_{a,b=1}^v \sum_q^{(\mathcal{I}_l)} \tilde{R}_{z \rightarrow (a,b)}^{(\ell)} N_{i,q}^{(\ell)}(a) N_{i+q,\lambda-q}^{(\ell)}(b) \\ &+ \sum_{a,b,c=1}^v \sum_{q,r}^{(\mathcal{I}_l)} \tilde{R}_{z \rightarrow (a,b,c)}^{(\ell)} N_{i,q}^{(\ell)}(a) N_{i+q,r}^{(\ell)}(b) N_{i+q+r,\lambda-q-r}^{(\ell)}(c) \end{aligned} \quad (71)$$

The initialization on unary splits  $\lambda = 1$  and the existence of only binary and ternary rules guarantees that  $N_{i,\lambda}^{(\ell-1)}$  can be nonzero only for  $\lambda \in I_{l-1}$ , i.e. the integer interval  $[2^{L-\ell+1}, 3^{L-\ell+1}]$ . In the first step of the hierarchy, corresponding to  $l = L$  in (71), the equation simplifies, as there is only one valid binary split for  $\lambda = 2$ ,  $q = 1$ , and one valid ternary split for  $\lambda = 3$ ,  $q = r = 1$ . This simplified form is given in the main text (Sec. 4, bullet point 4)

$$\begin{aligned} N_{i,\lambda=2}^{(L-1)}(z) &= \sum_{a,b} \tilde{R}_{z \rightarrow (a,b)}^{(L)} N_{i,1}^{(L)}(a) N_{i+1,1}^{(L)}(b) = \mathbf{1} \left\{ X_{i,\lambda=2}^{L-1} = z \right\}, \\ N_{i,\lambda=3}^{(L-1)}(z) &= \sum_{a,b,c} \tilde{R}_{z \rightarrow (a,b,c)}^{(L)} N_{i,1}^{(L)}(a) N_{i+1,1}^{(L)}(b) N_{i+2,1}^{(L)}(c) = \mathbf{1} \left\{ X_{i,\lambda=3}^{L-1} = z \right\}. \end{aligned} \quad (72)$$

Notice that, due to local ambiguity, these tensors do not identify the true nonterminals of the parse tree that generated the sentence  $\mathbf{X}$ , but only *candidate* nonterminals.

Multiplying Boolean tensors  $N_{i,\lambda}^{(\ell-1)}(z)$  that correspond to adjacent spans, we get indicator functions for pairs and triples of candidate nonterminals,

$$\begin{aligned} N_{i,\lambda,\lambda'}^{(\ell-1)}(a, b) &:= N_{i,\lambda}^{(\ell-1)}(a) N_{i+\lambda,\lambda'}^{(\ell-1)}(b), \\ N_{i,\lambda,\lambda',\lambda''}^{(\ell-1)}(a, b, c) &:= N_{i,\lambda}^{(\ell-1)}(a) N_{i+\lambda,\lambda'}^{(\ell-1)}(b) N_{i+\lambda+\lambda',\lambda''}^{(\ell-1)}(c), \end{aligned} \quad (73)$$

By measuring the covariances of these indicators with the root one-hot vector  $X^{(0)}$ , we get generalizations of  $C_2^{(L)}$  and  $C_3^{(L)}$ , that we can also average over all the possible starting positions  $i$  and span lengths  $\lambda, \lambda', \lambda''$  as the covariances in Eq. 2 and Eq. 3 are averaged over the starting position of the span of adjacent tokens.

We now show that the effect of spurious nonterminals on the level- $\ell$  covariances is negligible in the asymptotic vocabulary size limit, which justifies the procedure described in subsection 4.3. We will show this only for the covariance between pairs of spurious level- $(L-1)$  nonterminals and the root, but our conclusions extend immediately to all other cases and levels.

**True vs. spurious contributions (pair case).** Fix a start index  $i$  and a length pair  $(s, s') \in \{2, 3\}^2$ . Recall the adjacent-candidate indicator

$$N_{i,s,s'}^{(L-1)}(a, b) := \mathbf{1}\{X_{i,s}^{(L-1)} = a, X_{i+s,s'}^{(L-1)} = b\} \quad (74)$$

so that the root-to-pair moment is  $M_2^{(L)}(i, s, s'; (a, b), \alpha) = \mathbb{E}[N_{i,s,s'}^{(L-1)}(a, b)\mathbf{1}\{X^{(0)} = \alpha\}]$  and the corresponding covariance is

$$C_2^{(L)}(i, s, s') = \text{Cov}\left[N_{i,s,s'}^{(L-1)}, X^{(0)}\right] \in \mathbb{R}^{v \times v \times v}. \quad (75)$$

Let  $\tau$  denote the (random) parse tree, and let  $\{(t_k, s_k, X_k^{(L-1)})\}_{k=1}^K$  be the level- $(L-1)$  segmentation induced by  $\tau$ , where block  $k$  spans  $[t_k, t_k + s_k - 1]$ , has arity  $s_k \in \{2, 3\}$ , and carries latent  $X_k^{(L-1)}$ . Define the *true-adjacency event* at  $i$

$$A_i^{(s,s')} := \left\{ \exists k : t_k = i, s_k = s, t_{k+1} = i + s, s_{k+1} = s' \right\}. \quad (76)$$

On  $A_i^{(s,s')}$ , the two candidate spans coincide with two consecutive true level- $(L-1)$  nodes. We decompose (superscript  $L-1$  omitted to avoid clutter)

$$N_{i,s,s'}(a, b) = N_{i,s,s'}^{\text{true}}(a, b) + N_{i,s,s'}^{\text{spur}}(a, b), \quad (77)$$

where

$$N_{i,s,s'}^{\text{true}}(a, b) = N_{i,s,s'}(a, b) \mathbf{1}\{A_{i,s,s'}\}, \quad N_{i,s,s'}^{\text{spur}}(a, b) = N_{i,s,s'}(a, b) \mathbf{1}\{(A_{i,s,s'})^c\} \quad (78)$$

By linearity of covariance,

$$C_{2,(i,s,s')} = C_{2,(i,s,s')}^{\text{true}} + C_{2,(i,s,s')}^{\text{spur}}. \quad (79)$$

The term  $C_{2,i}^{\text{true}}$  is the *true* root-to-level- $(L-1)$ -pair covariance and the analyses of subsection C.2 applies.

**Conditioning on local topology and the law of total covariance.** To analyze  $C_2^{\text{spur}}$ , we condition on the local topology of the configuration. Let  $[i, i + s + s' - 1]$  be the window covered by the two adjacent candidates. Define  $\Gamma_i$  as the overlap pattern of the true level- $(L-1)$  segmentation restricted to  $I$ , i.e. the ordered list of true blocks intersecting  $[i, i + s + s' - 1]$ , together with their arities and whether they are truncated at the left/right boundaries. We choose  $\Gamma_i$  to be purely topological (i.e. it does not include the identities of nonterminals), so that it is independent of the root label  $X^{(0)}$ . Then the law of total covariance yields

$$C_{2,(i,s,s')}^{\text{spur}} = \mathbb{E}_{\Gamma_i} \left[ \text{Cov} \left[ N_{i,s,s'}^{\text{spur}}, X^{(0)} \middle| \Gamma_i \right] \right], \quad (80)$$

Fix a configuration,  $\Gamma_i = \gamma$ . Let  $\mathbf{k}_\gamma = (k_1, \dots, k_q)$  be the indices of the true level- $(L-1)$  blocks intersecting the interval  $[i, i + s + s' - 1]$  under  $\Gamma_i = \gamma$ , and set  $X_\gamma := (X_{k_1}, \dots, X_{k_q}) \in [v]^q$ . Define the probability

$$p_{\gamma, \mathbf{z}}(a, b) := \mathbb{P}\left(N_{i,s,s'}^{\text{spur}}(a, b) = 1 \mid \Gamma = \gamma, X_\gamma = \mathbf{z}\right), \quad \mathbf{z} \in [v]^q, \quad (81)$$

for the level- $(L-1)$  nonterminals  $\mathbf{z}$  and local topology  $\gamma$  to generate a span of terminals compatible with the pair of nonterminals  $(a, b)$ . Conditional on  $(\Gamma, Z_\Gamma)$ , the event  $\{N_{i,s,s'}^{\text{spur}}(a, b) = 1\}$  is conditionally independent of the root, therefore

$$\text{Cov} \left[ N_{i,s,s'}^{\text{spur}}, X^{(0)} \middle| \Gamma_i = \gamma, Z_\gamma = \mathbf{z} \right] = 0, \quad (82)$$

thus we may write the conditional spurious covariance as the weighted sum

$$\text{Cov} \left[ N_{i,s,s'}^{\text{spur}}(a, b), X^{(0)} \middle| \Gamma_i = \gamma \right] = \sum_{\mathbf{z} \in [v]^q} p_{\gamma, \mathbf{z}}(a, b) \text{Cov} \left[ \mathbf{1}\{Z_\gamma = \mathbf{z}\}, X^{(0)} \mid \Gamma = \gamma \right]. \quad (83)$$

Plugging back and averaging over  $\gamma$  gives the “true + spurious” decomposition with a fully local spurious term.

**Why the spurious term is negligible at large vocabulary size.** The last display shows that for fixed  $\gamma$  the spurious contribution is a sum over  $(\gamma, \mathbf{z})$  of *root-to-level- $(L-1)$ -nonterminals* weighted by  $p_{\gamma, \mathbf{z}}$ . In the random-rule ensemble defining the RHM, these atomic covariances behave like random variables over the choice of rules, and are (approximately) uncorrelated across distinct tuples  $\mathbf{z}$  unless they share the same underlying level- $(L-1)$  nonterminals. In addition, while the number of local topologies is finite, all the possible combinations of nonterminals  $\mathbf{z}$  have a positive (albeit small) probability of generating a sequence of terminals that overlaps with one of the possible derivations of the candidate pair  $(a, b)$ . As a result, the spurious term coincides with the average of at least  $\asymp v^2$ , uncorrelated terms proportional to the covariance between the root and  $\geq 2$  nonterminals. Due to the approximate uncorrelation, by a Central Limit Theorem argument, the average reduces the signal by the square root of the number of terms, i.e. by a factor at least  $O(v)$ , hence the spurious term is negligible.

### C.5. Sample complexity

Once the key data statistics entering the iterative algorithm have been identified (root-to-pair and root-to-triple covariances at all levels), we determine the sample complexity of the algorithm by studying the convergence of empirical estimates of such statistics to the corresponding population value. The covariance with the smallest typical size will be the one requiring the highest number of data to converge. Comparing Eq. 62 and Eq. 67 for arbitrary  $\ell$ , the covariance with the smallest size is

$$C_3^{(L)}((a, b, c), \alpha) = O\left(\frac{1}{fv^2} \sqrt{\frac{1}{v^3} \frac{(p_2^2/2)^{L-1}}{(fv)^{L-1}}}\right), \quad (84)$$

We compare this covariance with the typical sampling noise (standard deviation of the empirical estimator with respect to draws of a training dataset of size  $P$ )

$$\sqrt{\text{Var}[\widehat{C}_3^{(L)} - C_3^{(L)}]} = \sqrt{\frac{1}{(fv^2)v^2P}}, \quad (85)$$

where the factor  $v$  comes from the  $v$  possible root values and  $(fv^2)v = m_3v$  from the number of distinct triples that are valid ternary siblings. The comparison yields the complexity  $P^* = O(v(fv^2)(fv)^{L-1})$ , expressed in the main text as  $O(vm_3m_2^{L-1})$  to highlight the connection with the inverse root-to-triple correlations of the *easiest* branch leading to a triple of ternary siblings.

## D. Architectures and Training Details

We present here additional details regarding the neural network architectures and their training. As regards the input data, we represent RHM sequences as a one-hot encoding over the  $v$  token symbols. For the CNN and INN, we additionally whiten this  $d \times v$  tensor over the  $v$  channels, i.e. each of the  $d$  pixels has zero mean and unit variance across channels (Cagnetta et al., 2024).

### D.1. Convolutional neural networks (CNNs)

We build deep CNNs in the standard way by stacking convolutional layers. As noted in the main text, we choose a filter of size 4 and stride 2: this ensures that both rule types are always covered (i.e., all patches of length 2 and 3 are read by the filter). Mirroring the layered CFG, we apply a total of  $L + 1$  convolutional layers before reading off the label with a linear classifier. To handle sequences of varying length, we pad the input with zeros up to  $d_{max}(L) = 3^L$ , the maximum sequence length at depth  $L$  (for  $L = 2$  and  $L = 3$ , we in fact pad further to  $d = 10$  and  $d = 30$  respectively, to ensure the length of the feature map stays  $>4$  until the last layer). We have checked that padding with zeros in a symmetric manner, instead of adding zeros to the tail, does not change the results in any appreciable way.

As nonlinear activation function, we use the Rectified Linear Unit (ReLU) (whihout biases, as the input is whitened). The width (number of channels) per layer is set to  $H$ : we consider throughout the  $H \rightarrow \infty$ , overparametrized limit, with maximal update parametrization (Yang & Hu, 2021) to achieve stable learning. That is, we initialize weights as zero-mean unit-variance Gaussians, scale all hidden layers but the last by  $H^{-1/2}$ , scale the last layer by  $H^{-1}$  (to have vanishing output at initialization), and scale the learning rate with  $H$ . We find that the  $H \rightarrow \infty$  limit (in the sense that results are not changed by increasing further) is achieved by scaling according to the total number of ternary rules to be learned, in practice a safe

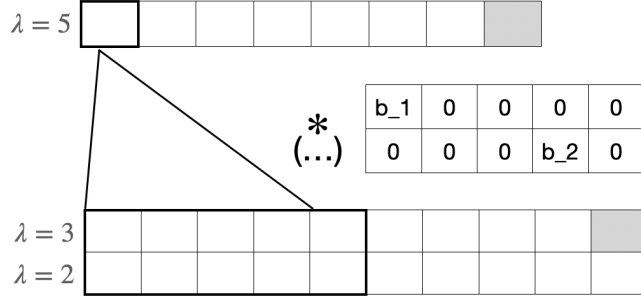


Figure 17. Sketch of the dilated filter corresponding to the binary split  $q = 3$  for  $\lambda = 5$ , i.e. splitting the substring of length 5 into two substrings 3-2. This is built by filling in the components of the base binary filter ( $b_1, b_2$ ) at the appropriate positions. The dilated filter is then convolved with the level- $(L - 1)$  feature map to build the  $\lambda = 5$  row of the level- $(L - 2)$  feature map (note one also has to convolve with the 2-3 filter, not shown, and sum the outputs).

criterion we find is  $H \sim 2vm_3 = 2fv^3$ . For most parameter values  $H = 1024$  more than suffices, while for the largest  $fv^3$  cases we increase this up to  $H = 2^{11}$  and  $2^{12}$ .

We consider standard Stochastic Gradient Descent (SGD) training on the cross-entropy loss, without momentum, learning rate set to  $H$  and batch size 128. For the general model with varying tree topology, due to the non-vanishing class entropy for any finite  $f$ , the training loss does not become arbitrarily small. We monitor the test loss and perform early stopping, by detecting a consistent rise or plateauing in the test loss. Once the training is stopped, we record the best model. Test loss data shown in the paper are obtained from averaging over 10 jointly independent realizations of grammar rules, sequences and weight initializations (same for INN, transformer below). The size of the test set is fixed in all cases to 20000: due to the combinatorial explosion of the total number of sequences  $P_{\max}$ , the probability of encountering a sequence seen during training in the test set is negligible.

## D.2. Inside neural network (INN)

We give here further details on the INN architecture. The basic idea is to use shared separate binary/ternary filters at each layer, and apply these in such a way as to construct feature maps which mirror the inside tensors of the inside algorithm (15). That is, at each level- $l$  we will build feature maps of size  $3^L \times (3^{L-l} - 2^{L-l} + 1) \times H$ , where the dimensions correspond to start positions (we pad the input with zeros up to  $d_{\max}(L) = 3^L$ ), span lengths  $\lambda \in \mathcal{I}_l$  (we will denote the total number of span lengths  $|\mathcal{I}_l|$  as  $N_\lambda(l) = 3^{L-l} - 2^{L-l} + 1$ ), and finally number of channels  $H$ . For classification we are interested only in the full span of the sentence, so that at the root level  $l = 0$  we consider only the first position  $i = 1$  and build a feature map of size  $(3^L - 2^L + 1) \times H$ . The final linear readout, which yields the logits over the  $n_c = v$  classes, is of the same size  $H \times n_c$  as in the CNN. This is thanks to the fact that we feed forward the sequence length  $d$  of each data point, and use dynamical indexing to read off only at the relevant position in the final feature map. The sequence length  $d$  can be calculated from the whitened input  $\tilde{x}$  as the sum of squares  $d = \sum_{i=1}^d \tilde{x}_i^2$ .

To build the level- $(l - 1)$  feature map from the level- $l$  map following the structure of (15), we will proceed by considering separate each value of the new span length  $\lambda \in \mathcal{I}_{l-1}$ . For a given  $\lambda$  we identify all the corresponding binary/ternary splits, i.e. all possible values  $\{q\}$  and  $\{q, r\}$  satisfying the constraints expressed in (15). For each binary/ternary split, we will build a *dilated* filter using the shared parameters of the base binary/ternary filter. To illustrate this, consider building the level- $(L - 2)$  map from the level- $(L - 1)$ , in particular for  $\lambda = 5$ . In this case there are two binary splits,  $q = 2$  and  $q = 3$ , corresponding respectively to splitting 5 as 2 – 3 or as 3 – 2. If we consider a 2D convolution, we will then want to construct e.g. the second of these ( $r = 3$ ) as a dilated filter by filling in the components of the base binary filter ( $b_1, b_2$ ) into a larger  $2 \times 5$  size filter which slides along the map below (see Fig. 17). We proceed analogously for ternary splits, filling in the base ternary filter ( $t_1, t_2, t_3$ ) at appropriate positions.

For efficient implementation, at each span length  $\lambda \in \mathcal{I}_{l-1}$  we first build all the relevant filters, stack them, perform all the convolutions in parallel and finally sum their outputs. This leaves a single loop over the span lengths  $\lambda \in \mathcal{I}_{l-1}$  to build the level- $(l - 1)$  feature map. In practice, in the code we first flatten the level- $l$  map into a linear  $N_\lambda(l) \times 3^L$  object by interleaving the span lengths, and perform 1D instead of 2D convolutions. In this representation, the kernel length of the dilated filters is  $N_\lambda(l) \times \lambda$ , and we perform 1D convolution with stride  $N_\lambda(l)$ ; for a binary split defined by  $q$ , we fill in the base filter ( $b_1, b_2$ ) at positions  $(q - 2^{L-l}, N_\lambda(l) \times q + \lambda - q - 2^{L-l})$  of the dilated filter, while for the ternary split  $q, r$  we

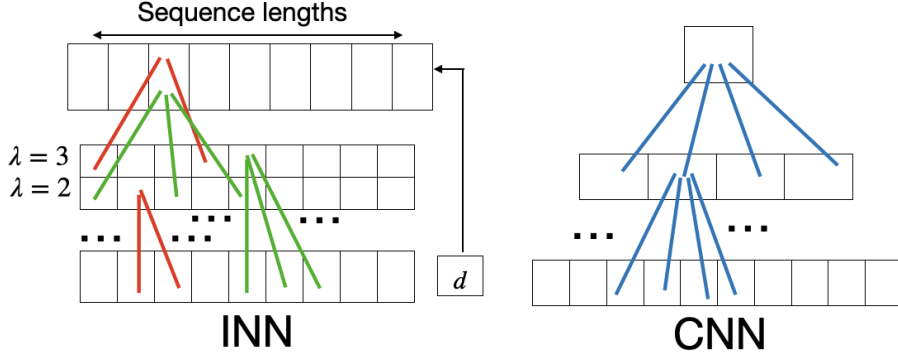


Figure 18. Sketch comparing the connectivity of the INN to the CNN for  $L = 2$ . While in the CNN we consider a single (shared) filter of length 4 and stride 2 at each layer, in the INN we consider separate shared binary/ternary (red/green) filters at each layer, which are applied to precisely build feature maps mirroring the inside tensors (15). The sequence length  $d$  is fed forward to the last layer (shown as example is  $d = 6$ , which receives input from the two parses  $3 - 3$  and  $2 - 2 - 2$ ).

fill in  $(t_1, t_2, t_3)$  at the three positions  $(q - 2^{L-l}, N_\lambda(l) \times q + r - 2^{L-l}, N_\lambda(l) \times (q + r) + \lambda - q - r - 2^{L-l})$ .

For initialization and training, we follow the same settings as in the CNN. In Fig. 18 we provide a sketch comparing the connectivity of the two architectures.

### D.3. Encoder-only transformer

We build transformers by stacking standard Multi-Head Attention layers (Vaswani et al., 2017) with layer normalization and multi-layer perceptron in between. The one-hot encoded input (padded with zeros up to  $3^L$ ) is firstly mapped into the embedding space of dimension  $d_{emb}$  by a learnable linear projection, to which we further add learnable positional embeddings. We choose  $d_{emb}$  and number of heads  $n_h$  large enough so that increasing them further does not improve performance, in particular  $d_{emb} = 512$  and  $n_h = 16$ . We make standard choices for the per-head width, set to  $d_{head} = d_{emb}/n_h$ , and the hidden size of the MLP,  $d_{mlp} = 4 \times d_{emb}$ .

We perform BERT-style classification in the standard way, by pre-pending a dummy [CLS] token to each sequence, which is one-hot encoded as an additional symbol in the vocabulary. To obtain the logits over the  $n_c$  class labels, we read out this initial position at the last layer. For training, we consider the same initialization as the CNN, but use instead an adam optimizer with learning rate tuned to  $5 \times 10^{-4}$ .

## E. Empirical signal-to-noise ratio (SNR)

We give here further details concerning the empirical signal-to-noise (SNR) measurement, which as stated in the main text we use to obtain an alternative  $P^*$  prediction which we can compare with the values extracted from CNNs (see Fig. 7(d)). Given that, as predicted by the theory, sample complexity is dominated by the task of grouping synonymous level- $L$  ternary rules, the SNR should reflect how the noisy correlations one would extract from a finite training set of size  $P$  approach their clean asymptotic values. Following this logic, we introduce the following quantity based on the conditional probability distribution across the class labels  $\alpha = 1, \dots, v$  given a triple  $(a, b, c)$  (which contains equivalent information to the covariances used in Sec. 4) at a specific position defined by  $I$ , i.e.

$$\text{SNR}_P((a, b, c)) = \frac{\|Pr(\alpha | (X_I=a, X_{I+1}=b, X_{I+2}=c)) - v^{-1}\vec{1}\|^2}{\|\hat{Pr}(\alpha | (X_I=a, X_{I+1}=b, X_{I+2}=c)) - Pr(\alpha | (X_I=a, X_{I+1}=b, X_{I+2}=c))\|^2} \quad (86)$$

where we choose  $I = \lfloor \langle s \rangle^L / 2 \rfloor$ , i.e. at the center of the typical sequence length, to avoid boundary effects.  $\hat{Pr}$  denotes the empirical estimate of this quantity after  $P$  samples. Note that in (86) we have the ratio of squared norms of two  $v$ -dimensional vectors: in the numerator, the ‘‘signal’’ measures how much the asymptotic values deviate from the uniform distribution  $v^{-1}$ , which would be the case if correlations were removed making the grammar unlearnable. In the denominator, the ‘‘noise’’ measures how much the empirical estimates deviate from the asymptote due to sampling noise. To obtain the final SNR, we average (86) across all grammatical triples (i.e. ternary rules)  $(a, b, c)$ .

In Fig. 19, we illustrate how we obtain the SNR  $P^*$  prediction for  $L = 3$ . For a range of training set sizes  $P$ , we firstly

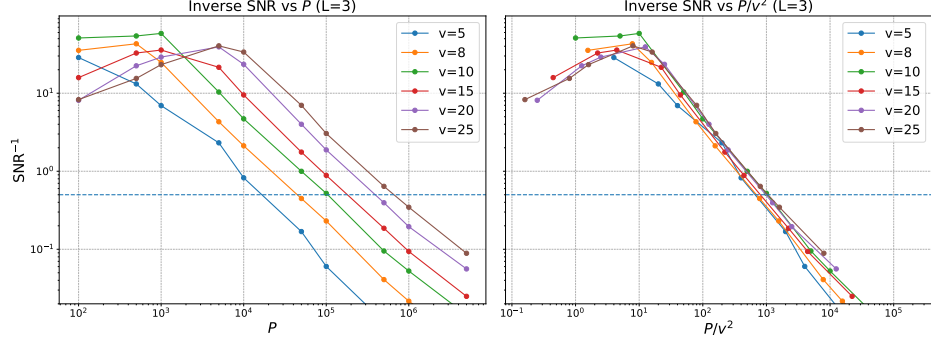


Figure 19. Inverse SNR curves  $SNR^{-1}(P)$ , computed at  $L = 3$  for different  $v$ , with  $f = 1/v$ . The dashed lines indicate the threshold  $SNR^{-1}(P^*) = 0.5$  which we set in order to extract the sample complexity prediction shown in Fig. 7(b).

extract the asymptotic probabilities, and for each  $P$  calculate (86) averaged across triples. We then fix a lower threshold on the inverse SNR curves, i.e.  $SNR^{-1}(P)$ , to obtain a sample complexity. Although there will be a dependence on the precise threshold value, for the reasonable choice  $SNR^{-1}(P^*) = 0.5$  we obtain an excellent agreement with the  $P^*$  from CNN data, as shown in Fig. 7(b).